The role of large-scale moistening by adiabatic lifting in the Madden-Julian Oscillation convective onset

Chelsea E. Snide

A Thesis submitted in partial fulfillment of

the requirements for the degree of

Master of Science

(Atmospheric and Oceanic Sciences)

at the

University of Wisconsin-Madison

August 2021

Abstract

The role of large-scale moistening by adiabatic lifting in the Madden-Julian Oscillation convective onset

by Chelsea E. Snide

The initiation of the Madden-Julian Oscillation over the Indian Ocean is examined through the use of a moisture budget that applies a version of the weak temperature gradient (WTG) approximation that does not neglect dry adiabatic vertical motions. Examination of this budget in ERA-Interim reveals that horizontal moisture advection and vertical advection by adiabatic lifting govern the moistening of the troposphere for both primary and successive MJO initiation events. For both types of initiation events, horizontal moisture advection peaks prior to the maximum moisture tendency, while adiabatic lifting peaks after the maximum moisture tendency. Once convection initiates, moisture is maintained by anomalous radiative and adiabatic lifting. Adiabatic lifting during successive MJO initiation is attributed to the return of the circumnavigating circulation from a previous MJO event, while in primary events the planetary-scale circulation appears to originate over South America. Examination of the same budget to data from the DYNAMO northern sounding array shows that adiabatic lifting contributes significantly to MJO maintenance in the DYNAMO data, with a contribution that is comparable to that of surface heat fluxes. However, results from the DYNAMO data disagree with those from ERA-Interim over the importance of adiabatic lifting to the moistening of the troposphere prior to the onset of convection. In spite of these differences, the results

from the two data sets show that small departures from WTG balance in the form of dry adiabatic motions are important for the maintenance of the moisture anomalies during MJO initiation.

Acknowledgements

The past two years have been difficult, unconventional and most importantly memorable. I am appreciative to everyone who has supported me along the way and contributed to my personal and academic growth. I would first like to thank my advisor, Dr. Ángel F. Adames, who provided invaluable insight and encouragement throughout this research project. I cannot express how appreciative I am for Dr. Ángel F. Adames along with the research group (Rosa Vargas-Martes, Haochang "HC" Luo, Kayleen Torres-Maldonado and Víctor Mayta) for their continued support and friendship. They have provided a lot of guidance and have truly made my time in graduate school memorable. I will always remember our conversations, group meetings, lunches/picnics and our shared obsession with coconut milk!

I am also grateful for my friendships with, Yingxiao Zhang, Chloe Whicker, Sakina Alblooshi, Poushali Ghoush and Karimar Ledesma-Maldonado. I have learned so much from you all and value your support!

Lastly, I would like to acknowledge Drs. Ángel F. Adames, Víctor C. Mayta and Scott W. Powell for their contributions to this research and help with my first publication. I want to thank Ángel F. Adames, for creating the schematic (Fig. 4.10), Víctor C. Mayta for his role in the DYNAMO analysis (Fig. 4.8 and Fig. 4.9) and Scott W. Powell for his insights on the decomposition of vertical motions. I want to also thank my committee members, Angela Rowe and Larissa Back for their insights and comments on this thesis work.

Contents

List of Figures

Chapter 1

Introduction

1.1 The Madden-Julian Oscillation

The Madden-Julian Oscillation (MJO, after Madden and Julian 1971, 1972) is an important mode of tropical intraseasonal variability. Studies often describe it as an envelope of convection thousands of kilometers across, coupled with planetary-scale circulations (Hendon and Salby, 1994, Kiladis et al., 2005). The associated circulation can be described in terms of wind patterns, where to the west of the convection there are low-level westerlies along with upper-level easterlies. This is connected to an overturning circulation. The convection usually develops over the western Indian Ocean in a process known as MJO initiation. Once initiated, the coupled convection and circulation features progress eastward at a rate of 5 m s^{-1} over the warm water of the Indo-Pacific warm pool (60°E–180°E) (Zhang, 2005). The convection often decays as it reaches the date

line, primarily due to cool sea surface temperatures, while the circulation and pressure oscillations continue propagating eastward at roughly 20-30 m s^{-1} (Hendon and Salby, 1994, Milliff and Madden, 1996, Sobel and Kim, 2012). The cycle of the MJO, including both the slowly-propagating convective signal over the warm pool and the fast circum-navigating signal, have profound impacts on the global circulation (Zhang, 2013) and are an important source of predictability at the intraseasonal timescale (Jiang et al., 2020, Kim et al., 2018). The MJO influences the variability of temperature and precipitation globally, modulates tropical cyclone activity and influences weather on a sub-seasonal to seasonal time frame (Zhang, 2005).

1.2   MJO Initiation

A salient feature of the MJO is that the circulation of a previous MJO event often returns to the Indian Ocean signaling the initiation of a "successive" convectively active phase of the MJO (Matthews, 2008, Powell, 2017). In other cases, the MJO becomes active in the absence of a circumnavigating signal, a process that is referred to as primary initiation (Matthews, 2008, Straub, 2013). The processes underlying both primary and successive MJO initiation are not well understood and pose an outstanding issue for simulating the MJO in Global Circulation Models (GCM) (Kim et al., 2018). To combat these uncertainties, the Dynamics of the Madden Julian Oscillation (DYNAMO) field campaign aimed to gather observational data for the initiation period. During the campaign, three successive events were observed over the Indian Ocean.

Based on the DYNAMO field campaign and model studies, various hypotheses have been proposed to understand the dynamics underlying MJO convective initiation. For successive MJO initiation, large-scale horizontal advection of moisture from the Maritime Continent has been suggested as the main moistening process (Li et al., 2015, Mei et al., 2015, Wolding, 2013, Zhao et al., 2013). Other studies have argued that the key process is free-tropospheric moistening by anomalous dry adiabatic lifting that results from the return of the circumnavigating signal to the Indian Ocean (Chen and Zhang, 2019, Haertel et al., 2015, Kikuchi and Takayabu, 2003, Powell, 2016, Powell and Houze Jr., 2015). These dry adiabatic motions are small, on the order of 1 mm s^{-1}, and are associated with temperature fluctuations on the order of $\sim$0.3 K (Powell, 2016) that have a maximum amplitude between 300 and 600 hPa. In spite of its small amplitude, anomalous upward dry adiabatic motions can suppress the background environmental subsidence, effectively moistening the free troposphere. Anomalous dry adiabatic lifting also increases the lower tropospheric lapse rate, so that convection becomes more likely to grow out of the boundary layer and moisten the free troposphere, allowing for extensive mesoscale regions of convection to occur (Powell, 2016, Powell and Houze Jr., 2015). For primary events it is argued that moistening in the lower troposphere over the Indian Ocean through nonlinear moisture advection is present prior to convective onset (Wei et al., 2019). Other studies focus on the suppressed convection anomaly as a precursor signal (Matthews, 2008, Yong, 2016), in-situ moistening by cumulus convection (Bellenger et al., 2015, Ruppert and Johnson, 2015), extratropical influences (Ray and Zhang, 2010), and equatorial waves (Takasuka et al., 2019).

1.3 The Weak Temperature Gradient Approximation

While the role of horizontal moisture advection in MJO initiation is well documented, there is little work quantifying the role of dry adiabatic lifting. Most studies that analyze the MJO-related moisture budget neglect the contributions from dry adiabatic lifting because of the conventional application of the weak temperature gradient (WTG) approximation (Sobel et al., 2001). In the WTG approximation, dry adiabatic vertical motions are neglected to leading order since they are much smaller than the vertical velocity that balances the diabatic heating associated with deep convection. WTG balance provides a picture of the mean state of the tropical atmosphere in which gravity waves eliminate temperature gradients through redistributing the heat produced by convection. The energy is able to be distributed across a large area primarily because Coriolis force is weak near the equator. This simplification has led to many advances in the understanding of tropical phenomenon and convection, however it does not fully capture the dynamics of the tropics (Adames et al. 2021). It is shown in observations that small temperature fluctuations play a role in the modulation of convection leading to a "relaxed" form of WTG approximation.

Moisture budgets that are examined through the conventional application of the WTG approximation neglect the moistening processes from dry adiabatic lifting (Chikira, 2014, Janiga and Zhang, 2016, Wolding et al., 2016). However, a recent study by Adames et al. (2021) found that the dry adiabatic lifting and diabatic vertical motions contribute roughly equally to the evolution of water vapor in the tropics. Although vertical moisture

advection from convective updrafts is much stronger than that arising from dry adiabatic lifting, it is largely cancelled out by drying from condensation. When the vertical moisture advection and condensation from convection are taken into account together, their net contribution to the evolution of water vapor is similar to that brought about from adiabatic lifting (Adames et al., 2021). Thus, it is possible that adiabatic lifting may play a central role in the convective initiation of the MJO, even when the atmosphere obeys the WTG approximation to leading order.

1.4   Research Questions

Through the application of a "relaxed" WTG moisture budget, a moisture budget can be derived that explicitly includes small temperature fluctuations and therefore dry adiabatic motions. Following the work done in (Adames et al., 2021), the evolution of moisture using this framework can be written in the following way:

$$L_v \frac{\partial q}{\partial t} + \mathbf{v} \cdot \nabla L q + \omega_Q \frac{\partial m}{\partial p} + L_v \omega_a \frac{\partial q}{\partial p} = 0 \tag{1.1}$$

Under the premise of a large-scale tropical environment, Eq. 1.1 can be scaled based off approximate values.

$$10^{-3} \ Jkg^{-1}s^{-1} \ + \ 10^{-3} \ Jkg^{-1}s^{-1} \ + \ 10^{-3} \ Jkg^{-1}s^{-1} \ + \ 10^{-3} \ Jkg^{-1}s^{-1} \ = 0 \tag{1.2}$$

Physically, this reveals that dry adiabatic lifting is on the same order of importance as diabatic processes for moisture evolution in the free troposphere of the tropical atmosphere. On the basis of the scale analysis, it is hypothesized that vertical moisture advection from dry adiabatic ascent plays an important role in MJO convective onset.

Although it is commonly assumed MJO initiations occur over the Indian Ocean, it was shown in Matthews (2008) that it only made up for 40% of total events. Based on those results, primary and successive events were identified for the Indian Ocean and Maritime Continent in order to look at convective onset. It is hypothesized that horizontal moisture advection will be strongest in Indian Ocean initiations, rather than Maritime Continent initiations. This is because the warm pool over the Maritime Continent promotes large amount of moisture and therefore pre-moistening would be less important in the case of Maritime Continent initiations. An analysis is then conducted to quantify the role of the following terms in Eq. 1.1 in order to answer the following questions:

- What are the predominant thermodynamic processes behind MJO convective initiation over the Indian Ocean?

- What role do adiabatic motions play in primary and successive MJO events?

- Do these results agree with those found in the DYNAMO field campaign?

- Are these processes different for initiations that occur over the Maritime Continent?

The results of this thesis are presented in Chapter 4 and 5 for initiations over the Indian Ocean and Maritime Continent respectively.

Chapter 2

Methods

2.1   Reanalysis and satellite data

Two datasets are used in this study. The first is the $1.5°$ longitude $\times$ $1.5°$ latitude horizontal resolution, four times daily fields from the European Centre for Medium-Range Weather Forecasts ERA-Interim reanalysis (ERA-I; Dee et al., 2011) for the 32-yr time period 1979 through 2010. We make use of the zonal, meridional and vertical winds (u, v, ω), specific humidity (q), temperature (T), diabatic heating rate (Q_1), surface and top of the atmosphere radiative fluxes, and surface sensible and latent heat fluxes (H and LE, respectively). The horizontal winds are used to calculate the velocity potential (χ) following Adames and Wallace (2014). The radiative fluxes are used to calculate the column-integrated radiative heating rate $\langle Q_r \rangle$. We will also calculate fields that are products of individual ERA-I variables. These products are calculated at each time step.

Spatial and temporal derivatives are calculated via a centered differences approach. The four times daily fields are averaged into daily means. Anomaly fields are obtained by removing the mean climatology at each point in space and time. The anomaly fields are then filtered using a Lanczos filter (Duchon, 1979) to retain only variability at the 20-100 day timescale.

In addition to the ERA-I data, we make use of 2.5° longitude × 2.5° latitude horizontal resolution, daily outgoing longwave radiation (OLR) from NOAA's polar-orbiting satellites (Liebmann and Smith, 1996) as an indicator of the extent of the high clouds associated with tropical deep convection.

2.2   Sounding observations from DYNAMO

To further analyze the moist process in the MJO initiation and verify the accuracy of the ERA-I reanalysis data, we used radiosonde measurements taken from the Dynamics of the Madden-Julian Oscillation (DYNAMO). We used data from the northern sounding array (NSA), located mostly north of the equator in the central equatorial Indian Ocean. Specifically, the NSA is defined by the following sites: Gan Island (0.69°N, 73.51°E); the R/V *Revelle* (0°, 80.5°E); Colombo (6.91°N, 79.878°E); and Malé (4.91°N, 73.53°E). Details of the sounding data, observing characteristics, and quality control procedures for DYNAMO sounding was documented in Ciesielski et al. (2014). In addition, a detailed description of the thermodynamic budget terms used in this study is documented in

Johnson et al. (2015). Different versions of the NSA DYNAMO data is available at `http://johnson.atmos.colostate.edu/dynamo/`, CSU version 3a was used for this analysis.

2.3   Identification and compositing of MJO initiation events

MJO activity is usually described via the use of an orthogonal pair of time series that describe the evolution of the MJO as it propagates around the equatorial belt. We will make use of the all-season OLR MJO Index (OMI; Kiladis et al., 2014) as our measure of MJO activity. The index is based solely on OLR data and thus more suitable to use to analyze the initiation of the MJO's convective signature over the Indian Ocean.

Our method for identifying MJO initiation events follows those of Matthews (2008), except MJO phases are defined using the OMI index. The standard MJO phase space is divided into four quadrants and assigned the following letters. Quadrant 'A' includes OMI phases 1 and 2, 'B' includes phases 3 and 4, 'C' includes 5 and 6, and 'D' includes 7 and 8 (Fig. 2.1). For the MJO to be considered active in these quadrants the amplitude of the OMI index, defined as $\sqrt{\text{OMI1}^2 + \text{OMI2}^2}$, must be greater than 0.8. If the MJO was inactive during this period, the letter 'N' is assigned instead. Our threshold for MJO activity is more strict than Matthews (2008) threshold of 0.4. However, our threshold is lower than the traditional threshold of an amplitude of unity. Our choice of an amplitude of 0.8 is a compromise between Matthews (2008) threshold, which captures a larger

amount of initiation events, and the standard definition of MJO activity, which would capture less but more robust activity.

A subset of MJO initiation events are defined as "primary". These are initiation events that occur in the absence of preceding MJO activity. Following the aforementioned lettering convention, primary events evolve in the MJO phase space following a letter pattern of NABCD, meaning there is no MJO activity prior to initiation. Successive events are defined as initiation events that occur while the OMI maintains an amplitude of 0.8 or greater, and hence evolve in the MJO phase space following the letter pattern DABCD. In this study we define the first day of MJO initiation over the Indian Ocean as the first day that is categorized as 'A' following 'D' and 'N' for successive and primary events, respectively. Following this method, we identify 25 primary and 52 successive MJO initiation events over the Indian Ocean. Additionally, initiations over the Maritime Continent are considered in this study. Using similiar constraints, the first day of initiation is categorized as 'B' following 'A' and 'N' for successive and primary events, respectively. There was 23 primary and 50 successive events identified for a Maritime Continent initiation. In this study, the primary events identified for both initiation locations are independent of each other, the successive events, however are not mutually exclusive.

Many of the plots shown in this study are lag composites of the primary and successive initiation events. In these composites, lag day 0 is defined as the first day of MJO initiation. Statistical significance of the composited fields is obtained from a two-tailed t-test under the null hypothesis that the composited fields are uncorrelated with the

evolution of the OMI during MJO initiation. The contour and shading in all the figures in this study are statistically significant at the 95% confidence interval.
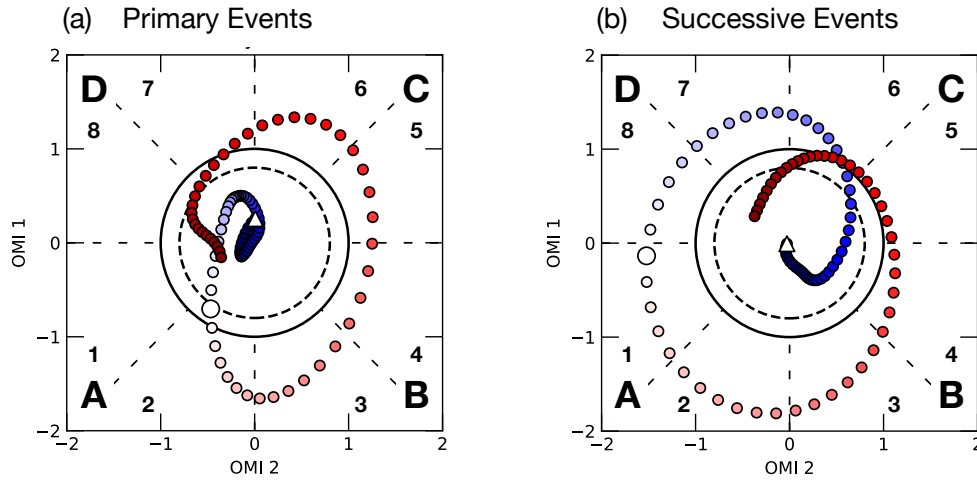
FIGURE 2.1: Composite phase space diagram of the OMI index for days -45 to 45 for (a) primary and (b) successive initiation events. The solid black circle represents an amplitude of 1.0. The dashed circle represents an amplitude of 0.8, the threshold necessary for events to not be categorized as 'N'. The white triangle marker denotes lag day -45 and the larger circle marker denotes lag day 0. The shading of the circles changes with increasing time, with darker blues indicating negative lags and reds indicating positive lags. The four quadrants and their corresponding MJO phases are shown in the corners of each panel.

Chapter 3

Moisture budget under the relaxed

WTG approximation

The equation that describes the conservation of specific humidity in isobaric coordinates can be written as

$$\frac{\partial Lq}{\partial t} = -\mathbf{v} \cdot \nabla Lq - \omega \frac{\partial Lq}{\partial p} - Q_2 \tag{3.1}$$

where L is the latent heat of vaporization, q is the specific humidity, $\mathbf{v}$ is the horizontal vector wind field, ω is the vertical velocity, and Q_2 the apparent moisture sink (Yanai et al., 1973). We can obtain more insight onto the processes that lead to the evolution of moisture during MJO initiation by following Adames et al. (2021) and Mapes (1997),

and decomposing the vertical velocity into a diabatic (ω_Q) and a dry adiabatic (ω_a) component:

$$\omega = \omega_Q + \omega_a \tag{3.2}$$

where the diabatic component satisfies WTG balance exactly

$$\omega_Q \frac{\partial s}{\partial p} \equiv Q_1 \tag{3.3}$$

where $s = c_p T + \Phi$ is the dry static energy, and Q_1 is the apparent heat source (Yanai et al., 1973). The dry adiabatic vertical velocity can be obtained as a residual $\omega_a = \omega - \omega_Q$. Alternatively, it can be estimated directly as proportional to the sum of the temperature tendency and the horizontal temperature advection term (Adames et al., 2021). We choose the former method because the calculation of both the temperature tendency and the horizontal advection require estimating derivatives, which introduces additional uncertainty to the estimation of ω_a.

Following Yanai et al. (1973), we can show that the difference between Q_1 and Q_2 describes the sum of radiative heating and the eddy flux convergence of eddy moist static energy (MSE):

$$Q_1 - Q_2 = Q_r - \frac{\partial \overline{\omega' m'}}{\partial p}. \tag{3.4}$$

where $m = C_p T + \Phi + Lq$ is the MSE. By separating the vertical velocity into its adiabatic and diabatic components and applying Eq. (3.4), we can column integrate Eq. (3.1) and write it as

$$\frac{\partial \langle Lq \rangle}{\partial t} = -\langle \mathbf{v} \cdot \nabla Lq \rangle - \left\langle \omega_a \frac{\partial Lq}{\partial p} \right\rangle - \left\langle \omega_Q \frac{\partial m}{\partial p} \right\rangle + \langle Q_r \rangle + LE + H \tag{3.5}$$

where the terms on the right-hand side are the column-integrated horizontal moisture advection, vertical moisture advection by adiabatic vertical motions, vertical MSE advection by diabatic vertical motions, column radiative heating and the surface latent and sensible heat fluxes, respectively. The vertical advection of MSE by ω_Q is the difference between vertical moisture advection by ω_Q and the apparent heat source

$$-\left\langle \omega_Q \frac{\partial m}{\partial p} \right\rangle = -\left\langle \omega_Q \frac{\partial Lq}{\partial p} \right\rangle - \langle Q_1 \rangle \tag{3.6}$$

where Eq. (3.3) is used to write Q_1 as a vertical DSE advection.

Chapter 4

Indian Ocean Initiation

4.1 Composite Primary and Successive Initiation

The evolution of the composited OMI index is shown in Fig. 2.1, for reference. In primary events, the amplitude of the OMI index reaches a value of 0.8 at lag day 0, and no activity is seen prior to this day. In contrast, during successive initiation events the amplitude of the OMI index exceeds a value of unity for ∼18 days prior to lag day 0. Both primary and successive initiation increase in amplitude after lag day 0, both reaching a maximum amplitude near lag day 8. Slow decay is observed thereafter, with the primary initiation event terminating near MJO phase 7 and the successive event decaying near phase 6. The overall evolution of the two types of initiation events closely follows that described by Matthews (2008). Of course, individual MJO cases within each composite may behave much differently than the mean.
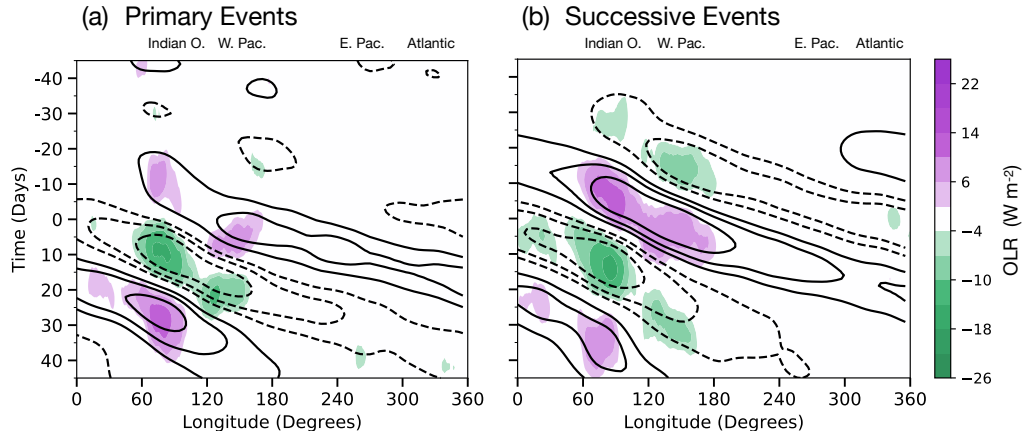
FIGURE 4.1: Hovmöller diagram of 20-100 day filtered anomalous outgoing longwave radiation (OLR) (shaded) and 150 hPa velocity potential (contoured) averaged over the 10°N/S latitude belt for (a) the lag composite of 25 primary MJO initiation events and (b) the composite of 52 successive initiation events. The ordinate shows the lag days from the time of initiation, with negative lags indicating days prior to the start of MJO initiation and positive lags indicating days after initiation. The contour interval is 10^5 m^2 s^{-1}.

Time-longitude (Hovmöller) diagrams of the primary and successive MJO initiation events are shown in Fig. 4.1a and 4.1b, respectively. During primary events, a weak positive OLR anomaly is seen collocated with a positive 150-hPa χ anomaly over the Indian Ocean at lag day -12. The OLR signal does not show any clear eastward propagation and decays by lag day -5 while the χ anomalies exhibit slow eastward propagation. Another positive OLR anomaly is seen near lag day 0 over the western Pacific (150°E-180°), in association with the eastward propagation of the 150-hPa χ anomalies. Near this time, a negative 150-hPa χ anomaly is observed propagating into the Indian Ocean from Africa, with negative OLR anomalies appearing at the time the χ anomalies reach the Indian Ocean. There is no evidence that these χ anomalies come from a previous MJO event. Instead, the anomalies appear to initiate over South America near 300° (120°W). Sakaeda and

Roundy (2016) showed that the upper-tropospheric Kelvin wave circulation associated with MJO initiation tends to develop in this region.

As the positive OLR anomalies decay, substantial amplification of the negative OLR anomalies occurs over the Indian Ocean, reaching a maximum amplitude near lag day 5. Unlike the positive OLR anomalies that precede it, the negative OLR anomalies exhibit a coherent pattern of eastward propagation up to lag day 25, where they decay near the date line.

In contrast to the primary initiation events, the successive events shown in Figure 4.1b show a coherent propagating signal that can be traced back to lag day -35. A succession of eastward-propagating positive and negative OLR anomalies can be seen from lag day -35, and they are organized into a pattern that is reminiscent of a wave train. These results are similar to those shown in Matthews (2008) but are shifted by about five days, largely a result of our choosing a different MJO index (see Table 2 in Kiladis et al., 2014 for more details).

A similar distinction between primary and successive events can be made by examining column-averaged ω_Q and ω_a. The evolution of OLR and ω_Q is shown for primary and successive events in Fig. 4.2a and 4.2b respectively. It is clear that diabatic vertical motions closely follow the OLR signal. The largest velocities are associated with deep convection and are largely confined to the warm pool. In both cases, ω_Q seems to originate over Eastern Africa. However, the signal in this region is more coherent and spatially coincides with a weak OLR signal in the successive events. In contrast, ω_a closely follows

the progression of the χ anomalies (Fig. 4.2c,d) around the world instead of appearing only where convection was active. For successive events (Fig 4.2d) we observe a signal in ω_a associated with the circumnavigating MJO signal (χ) that is seen propagating towards the Indian Ocean prior to MJO initiation. This signal can be traced back to the first MJO event in the sequence near lag day -35 and has a magnitude as large as -0.045 Pa s^{-1}. In contrast, a significant ω_a is not apparent until lag day 0 during primary initiation events. The noisy appearance of the ω_a signal near 30°E and 300° are likely the result of the Ethiopian Highlands and the Andes, respectively.

The results of Figs. 4.1 and 4.2 show a contrasting evolution of the OLR, ω_Q and ω_a field in the primary and successive MJO events. In order to understand the evolution of convection during MJO initiation, we analyze the terms that lead to the evolution of moisture in Eq. (3.5). For comparison, the column-integrated moisture anomalies are also shown (Fig. 4.3), which feature an evolution pattern that is reminiscent of the OLR anomalies in Fig 4.1. The top panel of Figure 4.3a shows that, during the initiation of primary events, moistening is seen over the Indian Ocean starting around lag day -5. The moisture tendency propagates eastward, showing a structure in the Hovmoller diagram that is reminiscent of the $\langle q \rangle$ anomalies, but shifted by about -10 lag days. For primary events, the moisture tendency prior to MJO onset does not extend to the west of the Indian Ocean, suggesting a weaker or non-existent circumnavigating signal.

Fig. 4.3b–d show the terms of the right-hand side of Eq. (3.5) that dominate the evolution of moisture during primary MJO initiation. These are horizontal moisture advection
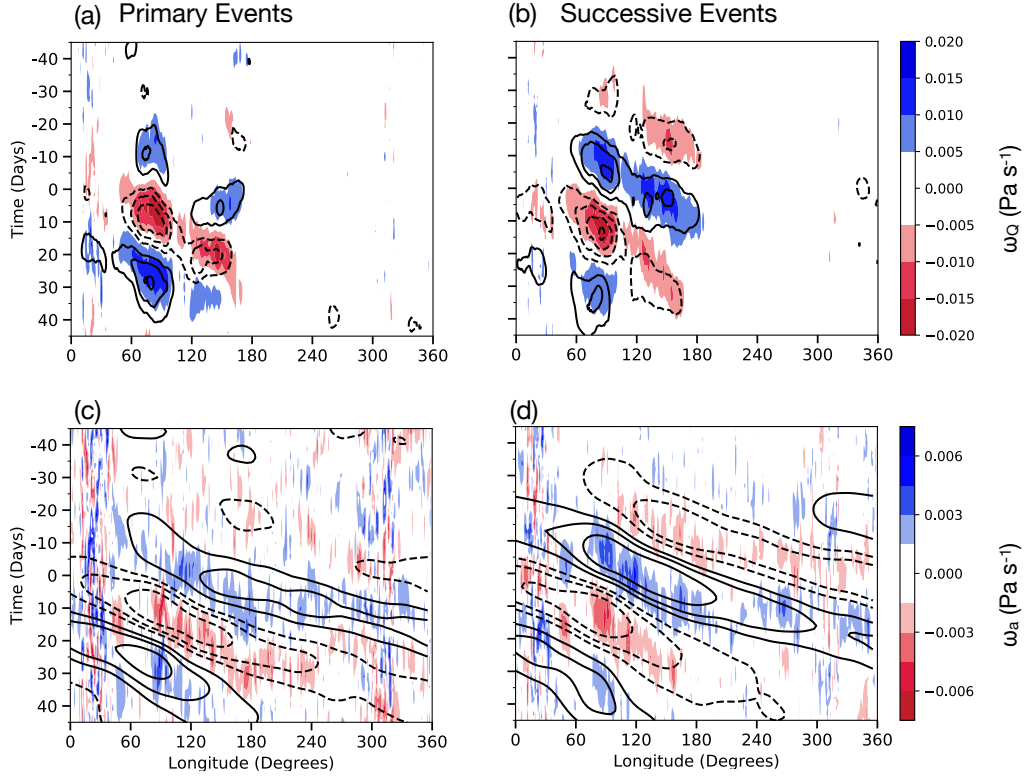
FIGURE 4.2: As in Fig. 2 but showing (top) 20-100 day filtered anomalous column average ω_Q (shaded) and OLR (contours) for (a) primary and (b) successive initiation events. (bottom) 20-100 day filtered anomalous column-averaged ω_a (shaded) and 150 hPa velocity potential (χ, contoured) for (a) primary and (b) successive initiation events. The contour interval is 4 W m^{-2} in the top panels and 10^5 m^2 s^{-1} in the bottom panels.

$(-\langle \mathbf{v}\cdot\nabla Lq\rangle)$, vertical advection of moisture by dry adiabatic vertical motions $(-\langle \omega_a \partial_p Lq\rangle)$ and vertical MSE advection by diabatic vertical motions $(-\langle \omega_Q \partial_p m\rangle)$. Horizontal moisture advection (Fig. 4.3b) exhibits a similar pattern to the moisture tendency, albeit noisier. In contrast, $-\langle \omega_a \partial_p Lq\rangle$ (Fig. 4.3c) and $-\langle \omega_Q \partial_p m\rangle$ exhibit a similiar amplitude to large-scale horizontal advection. However, the two processes are more in phase with the column moisture anomalies rather than the moisture tendency, suggesting that these processes are related to MJO maintenance. They also exhibit opposite polarities and

therefore tend to cancel one another, except away from the warm pool where $-\langle\omega_a\partial_p Lq\rangle$ is dominant. That $-\langle\omega_Q\partial_p m\rangle$ acts to dry the column during active MJO events is suggestive of stratiform convection (Inoue et al., 2020, Inoue and Back, 2015).
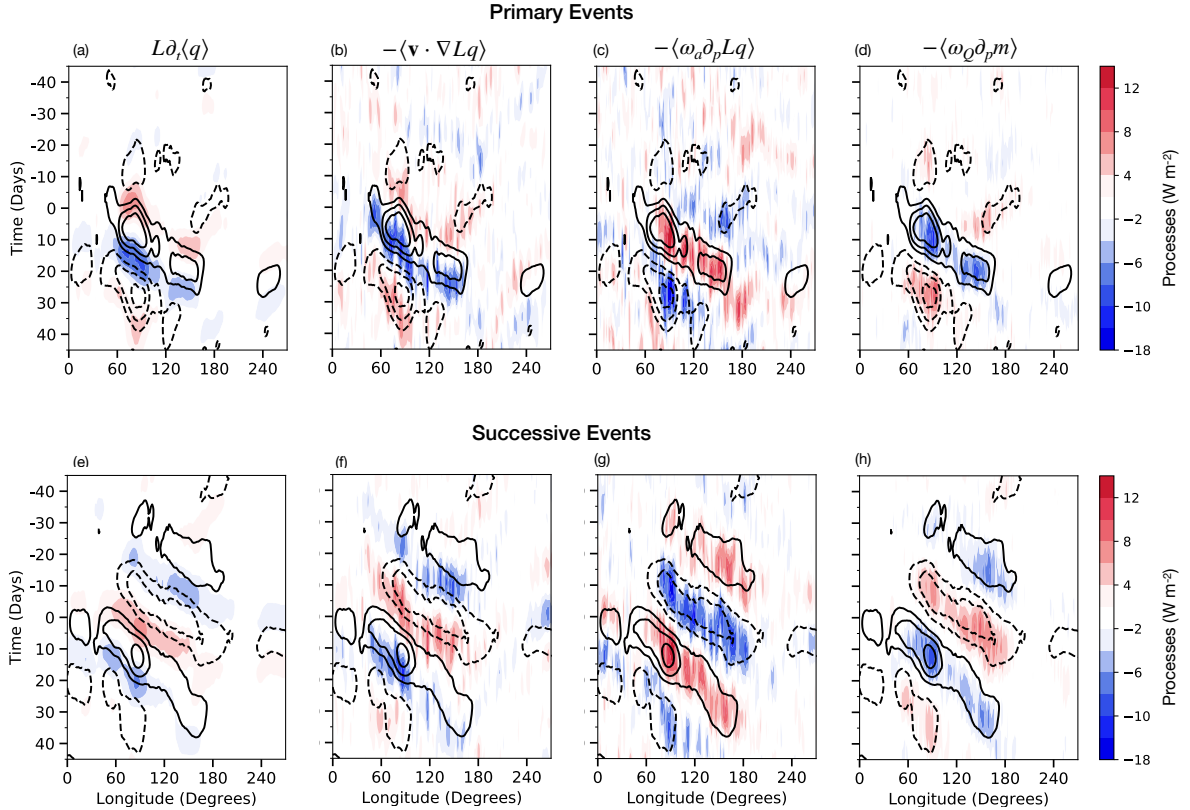
FIGURE 4.3: Hovmoller diagram of filtered (20-100 days) column integrated thermo-dynamic term anomalies (shading) and $\langle q\rangle$ anomalies (contoured) averaged over the 10°N/S latitude belt for both primary and successive events. (a) Moisture tendency term, (b) $-\langle\mathbf{v}\cdot\nabla Lq\rangle$, (c) $-\langle\omega_a\partial_p Lq\rangle$ and (d) $-\langle\omega_Q\partial_p m\rangle$. The contour interval for $\langle q\rangle$ is 0.5 mm.

In contrast to primary initiation events, the moisture tendency associated with the initiation of successive events (Fig. 4.3a, bottom) exhibits a coherent pattern of propagation as early as lag day -20 at 90°E, where an eastward-propagating drying tendency is observed. The drying is followed by eastward-propagating dry anomalies, which are then followed

by moistening near lag day -10. The moistening leading to successive MJO initiation occurs at the same lags that moistening occurs for primary MJO initiation. The relative amplitude of the processes that contribute to the moisture tendency during successive initiation are comparable to those occurring during primary initiation. However, in contrast to primary events, the moistening for successive events at lag day -5 extends all the way to eastern Africa ($\sim 0°$ longitude). Moistening by $-\langle \omega_a \partial_p Lq \rangle$ exhibits the largest amplitude over this region.

In order to more clearly quantify the evolution of the moist processes leading to MJO initiation, we average the moist processes in Fig. 4.3 over the Indian Ocean (10°N to 10°S and 60° to 100°E) and show them as line plots in Fig. 4.4. In these plots, lag day 0 is characterized by a maximum moistening tendency, indicating that MJO initiation is underway. For primary initiation events, horizontal moisture advection (green) peaks at lag day -5. Moistening by $-\langle \omega_a \partial_p Lq \rangle$ (blue) is a maximum near lag day 7, about the same time the $\langle q \rangle$ anomalies (black) reach their maximum amplitude. Radiative heating (orange) slightly lags $-\langle \omega_a \partial_p Lq \rangle$, peaking near lag day 9. Both $-\langle \omega_a \partial_p Lq \rangle$ and radiative heating are related to MJO maintenance, and largely counteract the drying from $-\langle \omega_Q \partial_p m \rangle$ (red). The offset between the terms is depicted in Fig. 4.4b by the purple line, which illustrates the sum of all terms on the right-hand side of Eq. (3.5).

Successive MJO initiation events exhibit a similar evolution in horizontal moisture advection albeit with a larger magnitude, which also peaks at lag day -5. Moistening by
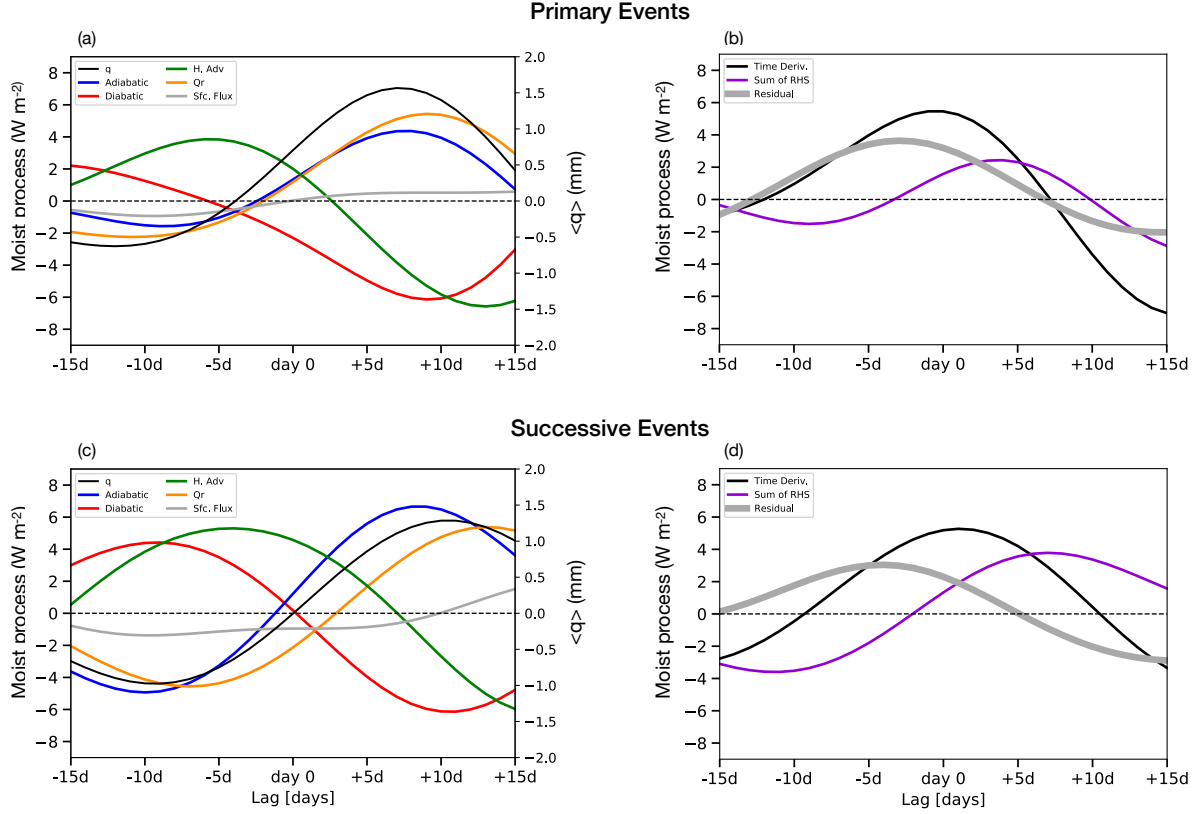
FIGURE 4.4: Lag composites of the column integrated moisture budget filtered for the MJO (20-100 days) and averaged over the Indian Ocean (10°N to 10°S and 60° to 100°) for (top) primary and (bottom) successive events. (a) Temporal evolution of $-\langle \omega_a \partial_p Lq \rangle$ (blue), $-\langle \omega_Q \partial_p m \rangle$ (red), horizontal moisture advection (green), radiative heating $\langle Q_r \rangle$ (orange), surface fluxes (gray) and column-integrated specific humidity (black). (b) Temporal evolution of the moisture tendency (black), the sum of all the right-hand-side terms in Eq. (3.5) (purple), and the budget residual (gray).

$-\langle \omega_Q \partial_p m \rangle$ is also seen from lag day -15 to lag day 0, in association with the preceding MJO suppressed phase. As in primary initiation events, $-\langle \omega_a \partial_p Lq \rangle$, $-\langle \omega_Q \partial_p m \rangle$ and $\langle Q_r \rangle$ all reach their maximum amplitude near the time when the $\langle q \rangle$ anomalies reach their maximum amplitude. However, there are some small shifts in the time these fields reach a maximum amplitude when compared to primary initiation events. For example, $\langle q \rangle$ reaches a maximum amplitude near lag day 10, compared to lag day 7 for primary events. Relative to the maximum in $\langle q \rangle$, the maximum in $-\langle \omega_a \partial_p Lq \rangle$ occurs at an earlier

time in successive initiation events, and its amplitude is $\sim 50\%$ larger than in primary initiation events. Conversely, $\langle Q_r \rangle$ and $-\langle \omega_Q \partial_p m \rangle$ shift in such a way that their phasing relative to $\langle q \rangle$ in successive initiation events is similar to that of primary events. The amplitude of these two processes is also similar for both types of MJO initiation.

When all the terms on the right-hand side in Eq. (3.5) are added together (purple line in Fig. 4.4b), we find that it is not equal to the moisture tendency. A residual in the moisture budget exists that exhibits an amplitude and structure similar to that found by Kim et al. (2014), being largely in phase with the horizontal moisture advection albeit with a slightly smaller amplitude. The signal is likely not related to the large-scale moisture advection. It is likely due to the analysis increments that exist in reanalysis data (Mapes and Bacmeister, 2012, Ren et al., 2021), which are related to an improper representation of convection and its interaction with moisture and radiation (Kim et al., 2014b, Yokoi, 2015).

Following Andersen and Kuang (2012), Adames (2017) and others, we can estimate the contribution of different processes to the initiation of the MJO by projecting the moist processes to the moisture anomalies and the moisture tendency, following the formula

$$\text{Proj}(X, \langle Lq \rangle) = \frac{||X \cdot \langle Lq \rangle||}{||\langle Lq \rangle \cdot \langle Lq \rangle||} \tag{4.1}$$

where $|| \cdot ||$ implies a sum over the Indian Ocean domain (10°N to 10°S and 60° to 100°), and from lag day -15 to 15, and X corresponds to any of the processes described

in Eq. (3.5). In previous studies, these projections would describe the contribution of moist processes to MJO maintenance $[\text{Proj}(X, \langle Lq \rangle)]$ and propagation $[\text{Proj}(X, \partial_t \langle Lq \rangle)]$. Since we are focused on MJO initiation in this study, $\text{Proj}(X, \partial_t \langle Lq \rangle)$ can be thought to describe the relative contribution of different processes to the moistening that leads to MJO initiation, while $\text{Proj}(X, \langle Lq \rangle)$ describes the relative contribution of different processes to the maintenance and amplification of the moisture anomalies during MJO initiation. Thus, chronologically-speaking, $\text{Proj}(X, \partial_t \langle Lq \rangle)$ describes the days prior to initiation while $\text{Proj}(X, \langle Lq \rangle)$ describes the days in which initiation is taking place.

For both primary and successive events, large-scale horizontal moisture advection is the largest contributor to moistening in the Indian Ocean (Fig. 4.5a,c), consistent with the results of Wolding (2013), Matthews (2008), and Zhao et al. (2013). Moistening by $-\langle \omega_a \partial_p Lq \rangle$ is the second-largest contributor. Both horizontal moisture advection and $-\langle \omega_a \partial_p Lq \rangle$ project more strongly onto the moisture tendency during successive MJO initiation than to primary. A major difference between successive and primary events is the positive role $\langle Q_r \rangle$ plays during primary propagation. This may be attributed to the convective structure of primary versus successive MJO events. The moistening that leads to MJO initiation is counteracted by drying by $-\langle \omega_Q \partial_p m \rangle$ for both primary and successive events. Suppressed surface energy fluxes also act to slow down moistening for successive initiation events.

The moisture anomalies during MJO initiation are maintained by $-\langle \omega_a \partial_p Lq \rangle$ and $\langle Q_r \rangle$ (Fig 4.5b,d). In primary events the two terms are comparable, with $\langle Q_r \rangle$ having a slightly

Primary Events

(a) Contribution to <q'> evolution (nondim)

(b) Contribution to <q'> maintenance (day^{-1})

Successive Events

(c)

(d)
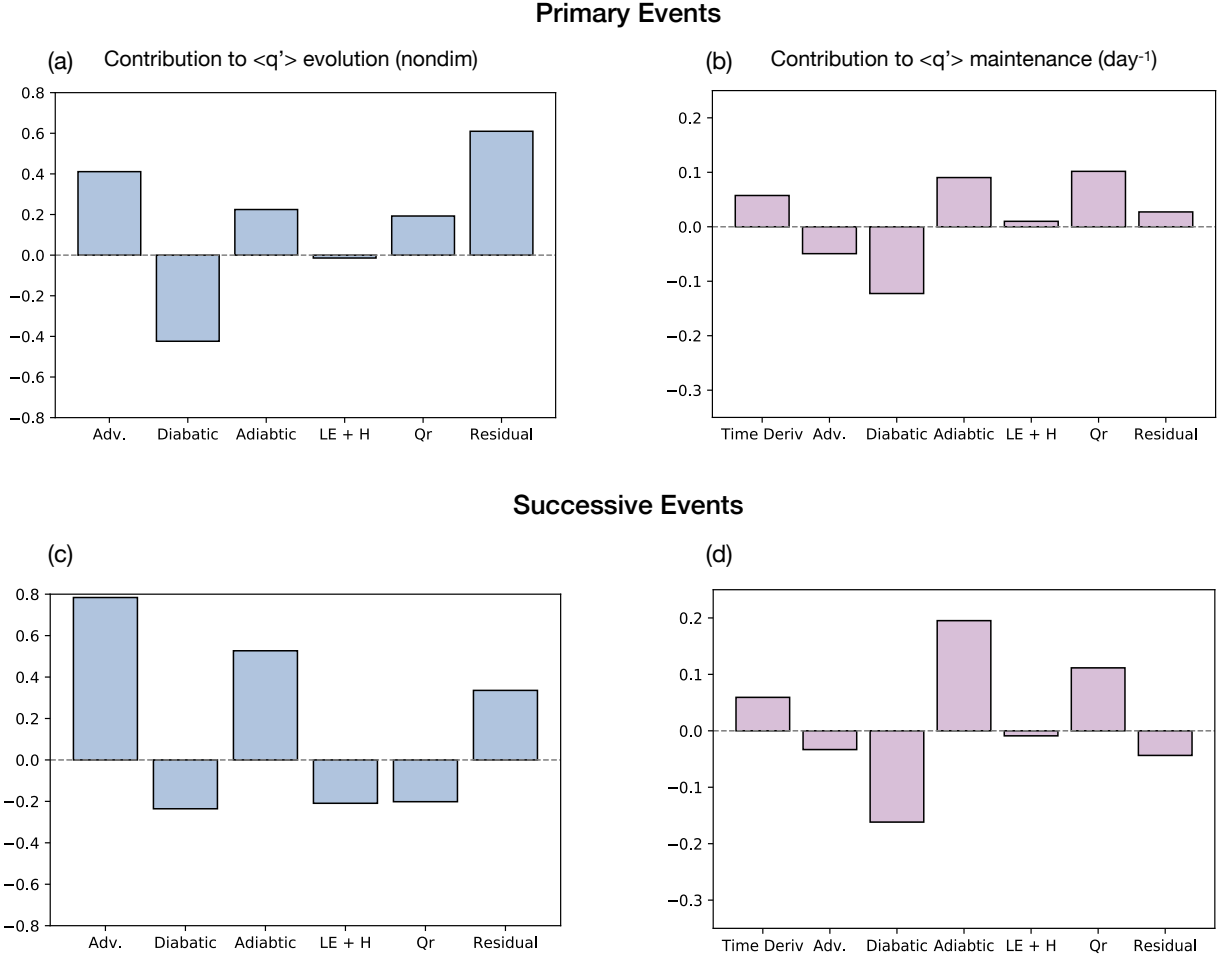
FIGURE 4.5: Fractional contribution of the thermodynamic budget in Equation (3.5) of moisture anomaly propagation and maintenance averaged over the Indian Ocean (10°N to 10°S and 60° to 100°E) for (a,b) primary events and (c,d) successive events. The projected terms are (from left to right): $\partial_t\langle Lq\rangle$, $-\langle \mathbf{v}\cdot\nabla Lq\rangle$, $-\langle \omega_Q\partial_p m\rangle$, $-\langle \omega_a\partial_p Lq\rangle$, $\langle Q_r\rangle$ and the budget residual.

larger contribution. However, in successive events $-\langle \omega_a\partial_p Lq\rangle$ contributes nearly twice as much to maintenance than $\langle Q_r\rangle$. Horizontal moisture advection and $-\langle \omega_Q\partial_p m\rangle$ act to damp the moisture anomalies, with the latter contributing a larger amount. The $-\langle \omega_Q\partial_p m\rangle$ is larger for successive events and contributes more to the damping than in primary events. That $\partial_t\langle Lq\rangle$ projects positively to the moisture anomalies indicates that the moistening terms exceed the drying terms, and the MJO is growing during this stage

of its life cycle.

The residual plays a positive role in both primary and successive propagation. It slightly leads the moisture tendency and follows a similar pattern to large-scale horizontal advection as seen in Fig. 4.4. The residual plays a larger role in primary event propagation and is the leading term. For anomaly maintenance the role of the residual is small but is positive in primary events and negative in successive events.

4.2   Sensitivity of ERA-I results to choice of domain

The intraseasonal column-integrated moisture budget of ERA-I and the DYNAMO northern sounding array during MJO initiation were compared. While the two data sets qualitatively agreed on which processes contributed to MJO maintenance and evolution, they also exhibited some marked differences. One difference is that the moist processes over the DYNAMO sounding array are nearly an order of magnitude larger than the ERA-I composites. Furthermore, the moisture tendency projects negatively to the moisture anomalies in the DYNAMO sounding data, implying damping, while it projects positively in the ERA-I data, implying growth. In this section we will show that some of the differences are attributed to the choice of averaging domain in Figs. 5 and 6.

Figure 4.6 shows the ERA-I budget terms from Fig. 4.4 but averaged over a smaller domain surrounding the DYNAMO sounding array location. By choosing a smaller domain we observe that the magnitude of the different terms compares more favorably to those from the DYNAMO array. However, they are still roughly half the amplitude.
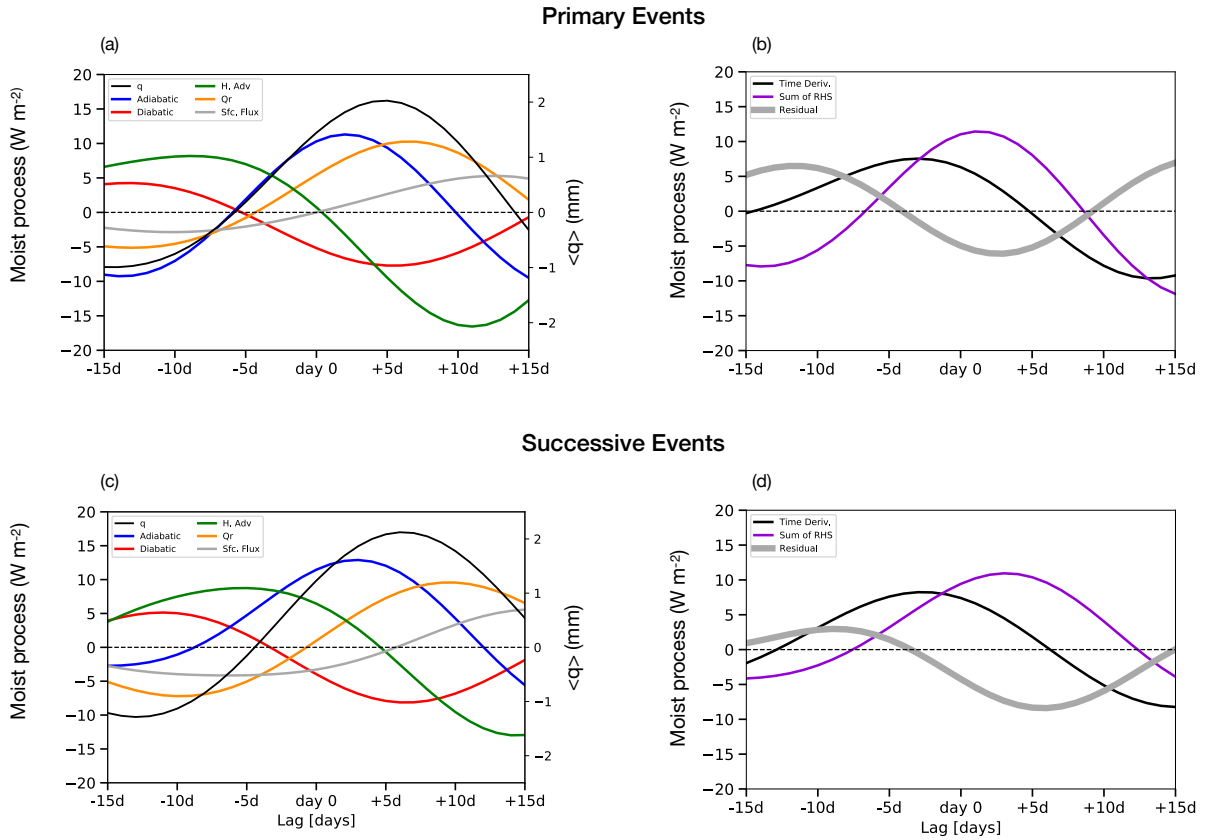
FIGURE 4.6: As in Fig 4.4 but averaged over the 3°N to 3°S and 70° to 75° domain.

This difference may be accounted for by the number of events that are composited in the ERA-I data (25 primary and 52 successive) versus the 3 events that were captured during DYNAMO.

In Figure 4.7 we also see that the projection of the moisture tendency on the moisture anomalies is no longer positive. The positive projection of the moisture anomalies in ERA-I is due to a correlation between the moisture and moisture tendency over the eastern Indian Ocean (80-100°E), to the east of the DYNAMO array. Thus, the moisture anomalies are likely growing during MJO initiation.

Primary Events

(a)   Contribution to <q'> evolution (nondim)

(b)   Contribution to <q'> maintenance (day⁻¹)

Successive Events

(c)

(d)
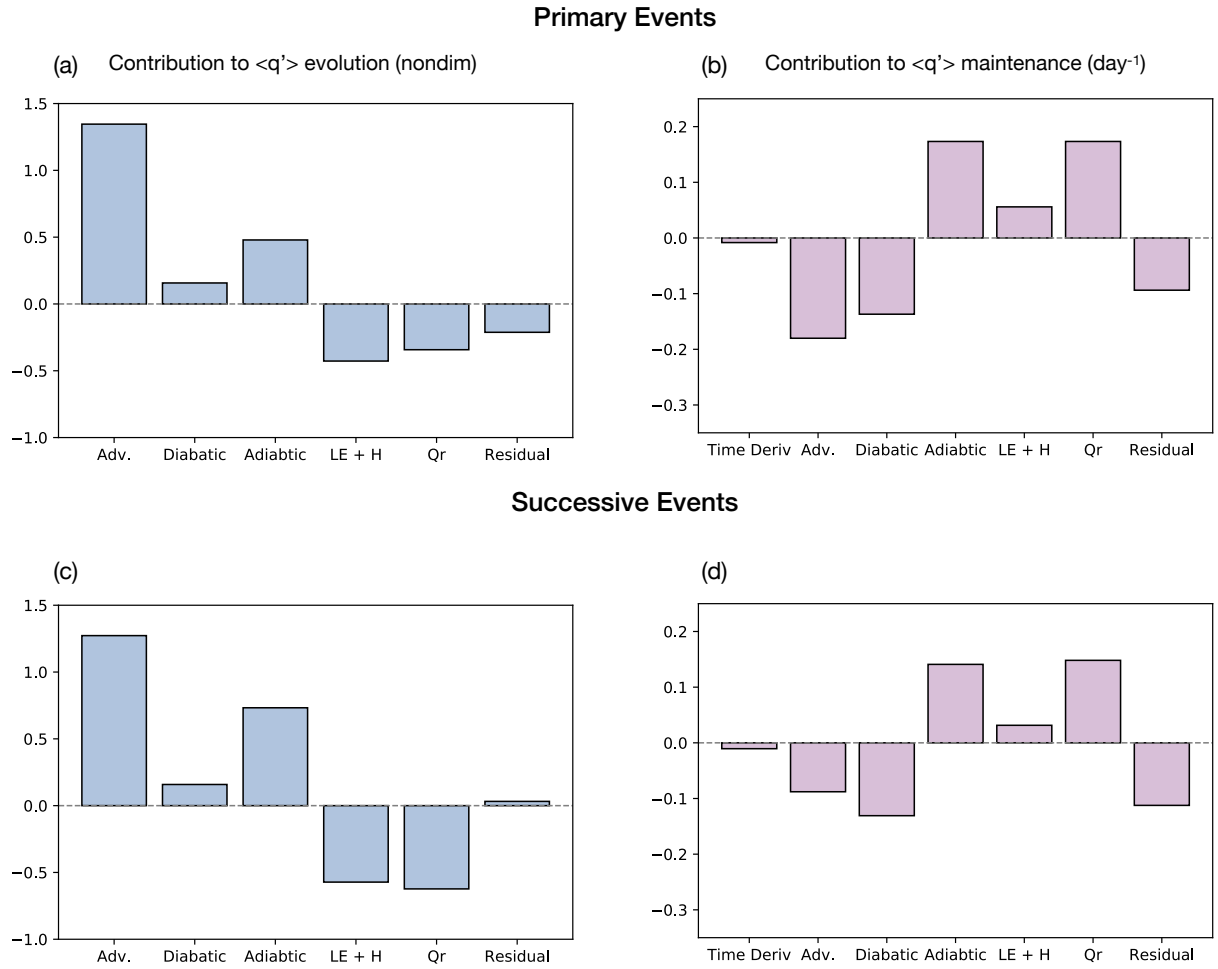
FIGURE 4.7: As in Fig. 4.5 but averaged over the 3°N to 3°S and 70° to 75° domain.

Looking at the progression of the budget terms in Fig. 4.6 averaged over the DYNAMO domain, the magnitude of $-\langle\omega_a\partial_p Lq\rangle$ is comparable to those seen in Fig. 4.8 and has a similar progression. A notable difference in ERA-I and DYNAMO data deals with the magnitude of $-\langle\omega_Q\partial_p m\rangle$, where reanalysis shows a smaller response. This is likely to do with misrepresentation of heating within ERA-I, and contributes to the residual seen in Fig. 4.6b,c. It is made clear that the adiabatic term in both datasets plays a role in offsetting the drying due to condensation processes and without it the moisture tendency

would be smaller.

In Fig. 4.7 the contribution to the evolution and maintenance of moisture anomalies during MJO initiation can be visualized. As seen in the the DYNAMO data projections (Fig. 8b in the main text) the time derivative is projecting negatively implying drying, this same signal can be seen in ERA-I when analyzing a smaller domain. The largest difference that remains is the sign of $-\langle \omega_a \partial_p L q \rangle$ in the evolution of moisture anomalies.

4.3   Role of ω_a in MJO initiation during DYNAMO

Model and numerical errors largely contribute to the residual (Fig. 4.4 and Fig. 4.5) found in the reanalysis data (Mapes and Bacmeister, 2012, Ren et al., 2021). To further examine the validity of Figs. 4.4–4.5, we compared these results to those of a sounding-based moisture budget from observations collected during the DYNAMO field campaign. Since the observational analysis is limited to three MJO events, Fig. 4.8 is calculated using linear regression analysis. In other words, we regressed moisture budget terms of Eq. (3.5) against the OMI1 MJO index. This deviates from the methodology found in Matthews (2008) and what was used in the reanalysis composites, although the results are interpreted in the same way as ERA-I composites. Based on the methodology for identifying primary and successive events, the three DYNAMO events are representative of successive initiations.

Examination of Fig. 4.8 reveals that horizontal moisture advection and $-\langle \omega_Q \partial_p m \rangle$ moisten the atmosphere prior to MJO initiation. The moistening is partly offset by

anomalous radiative cooling, suppressed surface fluxes and drying by $-\langle \omega_a \partial_p Lq \rangle$. As the moisture anomalies increase, these processes reverse polarity. At the time when the $\langle q \rangle$ anomalies attain their maximum amplitude we observe that surface fluxes, radiative heating and $-\langle \omega_a \partial_p Lq \rangle$ are positive, suggesting that these processes play a role in MJO maintenance. Moistening from $-\langle \omega_a \partial_p Lq \rangle$ is roughly of equal importance as surface fluxes in maintaining the convection.

The results from the DYNAMO soundings qualitatively agree with the composites made from ERA-I data, although the processes in the former are nearly an order of magnitude larger than the latter. In both data sets $-\langle \omega_a \partial_p Lq \rangle$ peaks after the maximum in the moisture tendency occurs and approximately out of phase with $-\langle \omega_Q \partial_p m \rangle$. Additionally, it is clear that in both data sets $-\langle \omega_Q \partial_p m \rangle$ and horizontal moisture advection are the dominant contributors to the moisture tendency.

However, there are some notable differences between the DYNAMO and ERA-I datasets. In the DYNAMO data, $\langle Q_r \rangle$ and $-\langle \omega_Q \partial_p m \rangle$ are larger in comparison to the moisture tendency than they are in reanalysis. Another significant difference is the larger role surface fluxes play in the DYNAMO data, which play a negligible role in the reanalysis. In both cases however, $-\langle \omega_a \partial_p Lq \rangle$ is roughly the same magnitude as the moisture tendency. We show that some of the differences between ERA-I and DYNAMO can be attributed to the domain averaging used in the reanalysis data.

One disadvantage of the use of Eq. (3.5) is that radiative heating contributes to $-\langle \omega_Q \partial_p m \rangle$

due to the large-scale circulations that $\langle Q_r \rangle$ produces in order to satisfy the WTG approximation (Adames and Maloney, 2021, Wolding et al., 2016). However, the DYNAMO data allows us to quantify the contributions of radiative and convective heating to ω_Q. Following Adames et al. (2021), we rewrite the sum of radiative heating and $\langle \omega_Q \partial_p m \rangle$ as

$$-\left\langle \omega_Q \frac{\partial m}{\partial p} \right\rangle + \langle Q_r \rangle = -\left\langle \omega_c \frac{\partial m}{\partial p} \right\rangle - \left\langle \omega_r \frac{\partial Lq}{\partial p} \right\rangle \qquad (4.2)$$

where the terms on the right-hand side are the vertical MSE advection by convective vertical motions (ω_c) and the vertical moisture advection by radiative vertical motions (ω_r). It is worth noting that the terms on the right-hand side of Eq. (4.2) fully separate the contribution of convection and radiation to the column moisture tendency.

The terms on the right hand side of of Eq. (4.2) are regressed onto the OMI1 time series as was done with the terms of Eq. (3.5). When we examine the contributions of $-\langle \omega_c \partial_p m \rangle$ and $-\langle \omega_r \partial_p Lq \rangle$ to MJO initiation (bottom panel of Fig. 4.8), we find that the former is nearly identical to $-\langle \omega_Q \partial_p m \rangle$ and the latter to $\langle Q_r \rangle$, except they are shifted by roughly 2-3 days. Thus to a first approximation we can interpret $-\langle \omega_Q \partial_p m \rangle$ as describing the net moistening by convective motions and $\langle Q_r \rangle$ as describing the moistening of the troposphere by radiative heating.

Lastly, it is instructive to estimate the contribution of the moist processes calculated from the DYNAMO sounding array to the maintenance and evolution of the moisture anomalies (Fig. 4.9). When it comes to the processes that lead to the evolution of the
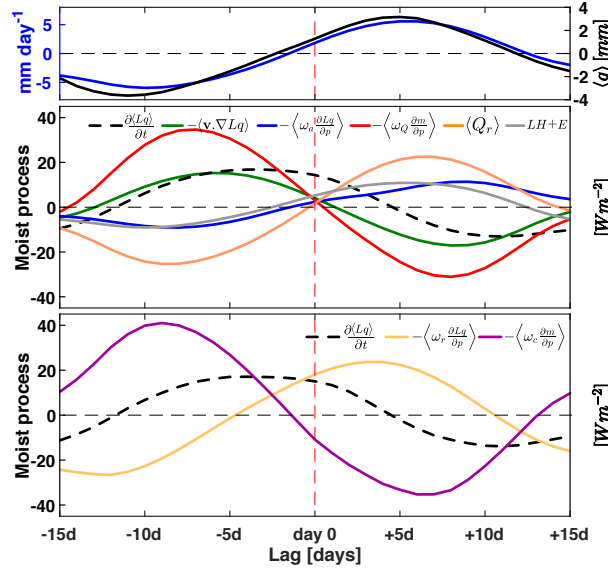
FIGURE 4.8: Lag regression based on the OMI1 time series and moisture budget terms calculated over the DYNAMO northern array. The top panel shows TRMM-3B42 rainfall rate (blue), and column moisture (black). (middle) Regressed anomalies of moisture budget terms of Eq. (3.5): $\partial_t \langle Lq \rangle$ (dashed black), $-\langle \mathbf{v}.\nabla Lq \rangle$ (green), $-\langle \omega_a \partial_p Lq \rangle$ (blue), $-\langle \omega_Q \partial_p m \rangle$ (red), $\langle Q_r \rangle$ (orange), and surface turbulent flux $LE + H$ (gray). (bottom) Regressed anomalies of moisture budget terms of Eq. (4.2): $-\langle \omega_c \partial_p m \rangle$ (purple), and $-\langle \omega_r \partial_p Lq \rangle$ (yellow).

moisture anomalies, there are more notable differences between the sounding data and ERA-I. The term $-\langle \omega_a \partial_p Lq \rangle$ does not significantly contribute to the propagation in the sounding data. Furthermore, $-\langle \omega_Q \partial_p m \rangle$ contributes more to the moisture tendency than horizontal moisture advection does in the sounding data, which is in stark contrast to ERA-I. This difference cannot be accounted for even if all of the residual in Fig. 4.5 were allocated to $-\langle \omega_Q \partial_p m \rangle$.

When it comes to the processes that maintain the moisture anomalies, it is seen that $-\langle \omega_a \partial_p Lq \rangle$ contributes roughly the same amount to MJO maintenance as it does in the ERA-I composites. However, the fractional contributions of $-\langle \omega_Q \partial_p m \rangle$ and $\langle Q_r \rangle$ are roughly twice as large in the sounding data than in ERA-I. The time derivative also

projects weakly negatively to the moisture anomalies. Lastly, as expected, the residual in the sounding data is much smaller than that found in ERA-I data, and negligible in comparison to the other fields.
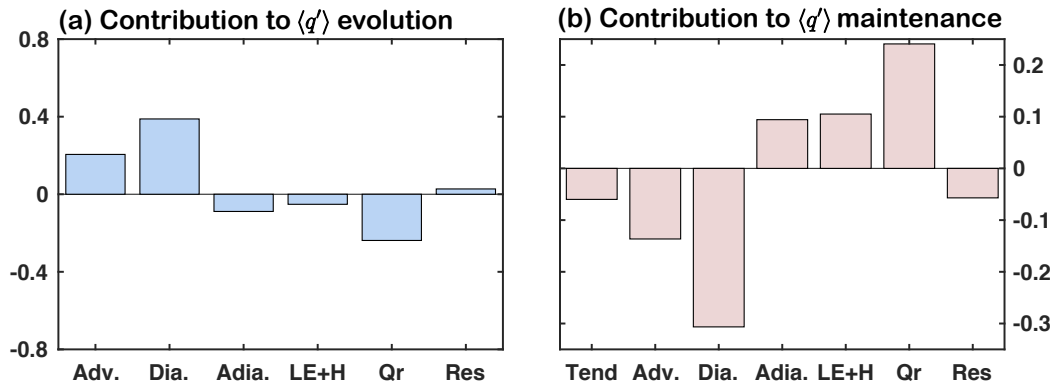
FIGURE 4.9: As in Fig. 4.5, but for data from the DYNAMO northern sounding array.

4.4 Discussion

In the preceding sections, we sought to understand the processes that lead to moistening of the troposphere during primary and successive MJO initiation events over the Indian Ocean. Unlike previous studies, we quantify the role of large-scale dry adiabatic lifting during MJO initiation by employing a "relaxed WTG" moisture budget (Adames et al., 2021). On the basis of a composite analysis similar to that of Matthews (2008) but using the OLR MJO index (OMI) (Kiladis et al., 2014) in ERA-I data, we find that large-scale horizontal advection plays a critical role in the moistening of the troposphere during the days leading up to primary and successive MJO initiation, as suggested by previous studies (Li et al., 2015, Wolding, 2013, Zhao et al., 2013). For successive initiation, we interpret this moistening as the result of anomalous easterlies associated with a previous MJO suppressed phase advecting moist air from the Maritime Continent, as previous

studies have shown (Nasuno et al., 2015, Zhao et al., 2013). Suppressed convection also exists prior to primary MJO initiation, and it is possible that it aids the onset of the active MJO by moistening the troposphere through horizontal moisture advection. Nonlinear moisture advection could also play a major role in both primary and successive initiation events, as suggested by Nasuno et al. (2015) and Wei et al. (2019).

We also find that vertical moisture advection by adiabatic lifting is of leading-order importance for the initiation of both primary and successive events (Fig. 4.5). Large-scale horizontal moisture advection and dry adiabatic lifting are of comparable magnitude but large-scale horizontal advection peaks prior to initiation while adiabatic motions become more important as convection is increasing over the Indian Ocean, as shown in Fig. 4.4. Because dry adiabatic lifting peaks as the convection is increasing over the Indian Ocean, we also find that this process plays a significant role in MJO maintenance. Its role in maintenance is comparable to that of radiative heating in primary initiation events, while it is larger for successive events. While it is well-known that radiative heating plays an important role in MJO maintenance (Andersen and Kuang, 2012, Kim et al., 2014, Sobel et al., 2014), the importance of dry adiabatic lifting in MJO maintenance has not been previously documented.

By synthesizing Figures 4.1–4.9, we can obtain a clearer picture of the sequence of events that lead to MJO initiation over the Indian Ocean, as shown schematically in Fig. 4.10. In successive events, a circumnavigating signal is seen in the χ anomalies that are traced back to a previous active MJO event that was propagating over the warm pool during
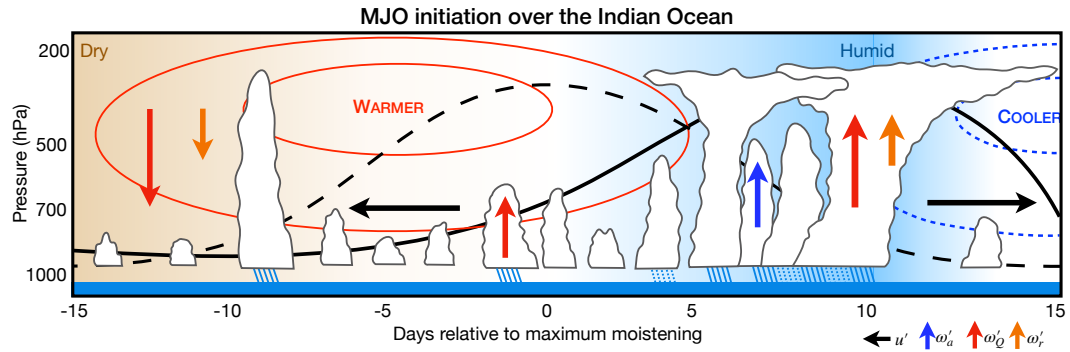
FIGURE 4.10: Schematic describing the temporal evolution of moistening process of a composite MJO initiation event over the Indian Ocean. The solid line denotes the column moisture anomalies while the dashed line denotes the moisture tendency. Arrows depict the horizontal wind and the adiabatic, diabatic and radiative vertical velocities with colors indicated by the legend. Solid red contours denote warm anomalies while dashed blue contours depict cold anomalies. The light blue background denotes a humid troposphere while the light brown background denotes a dry troposphere.

lag days -25 to -10. The circumnavigating signal returns to the Indian Ocean near lag day 5, coinciding with the increase in dry adiabatic lifting over this region. This lifting reinforces the moistening tendency over the Indian Ocean, which had been governed by horizontal moisture advection up to that point (Fig. 4.3). In primary events, the origin of the χ anomalies are not related to a prior MJO event, but instead can be traced to South America ($\sim300°$ longitude). A similar result was found by Sakaeda and Roundy (2015, 2016), who found that an equatorial wave signal reminiscent of a Kelvin wave is excited in South America which then propagates eastward towards the Indian Ocean. The dry adiabatic lifting associated with this wave coincides with the increase in moisture over the Indian Ocean, suggesting that it acts to maintain it. Although moistening by adiabatic lifting plays a role in both types of initiation events, this process is nearly twice as strong in successive initiation events, likely due to the strength of the circumnavigating signal, as suggested by the χ contours in Fig. 4.1.

In spite of the difference in origin and magnitude of the dry adiabatic lifting, the evolution of primary and successive events is broadly similar, and thus Fig. 4.10 can be used to summarize both types of initiation. Moistening of the Indian Ocean begins as a result of anomalous horizontal moisture advection, followed by moistening by adiabatic lifting. Once convection develops, both dry adiabatic lifting and radiative heating maintain the moisture anomalies from dissipating from increased condensation from the enhanced deep convection.

Because the ERA-I data contains a substantial residual in the moisture budget analysis, we compared the results from ERA-I with sounding-based data from DYNAMO. While the two data sets qualitatively agree on the role of the moist processes in MJO evolution, they also exhibit marked differences. Many of these differences are attributed to the compositing method. The ERA-I results are based on composites that span the equatorial Indian Ocean (60-100°E, 10°N/S), while the DYNAMO data is limited to the northern sounding array. The differences attributed to compositing method include the overall magnitude of the processes, the role of surface fluxes in MJO maintenance, and the projection of the moisture tendency on the moisture anomalies. We discuss these differences in further detail in the Supplementary Material. However, several differences between ERA-I and DYNAMO cannot be explained by choice of methods. For example, vertical MSE advection by diabatic heating plays a primary role in MJO evolution in the DYNAMO data, while its contribution is negligible in ERA-I. Furthermore, dry adiabatic lifting is not found to play a significant role in the moistening prior to the onset of convection in the DYNAMO data (Fig. 4.9b), while it is the second largest contributor

in ERA-I. It is possible that these differences can be partly attributed to the budget residual in ERA-I and the fact that ERA-I is a composite of multiple MJO events while the DYNAMO data only contains 3 events. However, more work is needed to further understand these disagreements between the datasets.

The results from both ERA-I and DYNAMO data exhibit some similarities to the findings of Powell (2016). In his study, adiabatic motions were suggested to play a significant role in the temperature tendency associated with initiation, which played a key role in the moistening of the free trosposphere during a single MJO initiation. We note, however, that Powell (2016) defined adiabatic lifting as the vertical DSE advection by the total vertical velocity, including the vertical velocities that balance the diabatic heating. Furthermore, his thermodynamic budget is evaluated on data with mean fields retained, while our budget is filtered to retain intraseasonal variability. In spite of these differences, examination of Figs. 16 and 17 in Powell (2016) shows a cooling of the troposphere during MJO initiation, consistent with the adiabatic lifting that is found in this study.

While our results suggest a chronological order in the processes that lead to MJO initiation, our results do not invalidate different views on MJO initiation. It is possible that extratropical forcing could lead to dry adiabatic lifting over the Indian Ocean, or that extratropical motions can excite the wave signal that leads to primary initiation (Ray and Zhang, 2010, Sakaeda and Roundy, 2016). Additionally, the horizontal moisture advection can come from intraseasonal circulation features (Zhao et al., 2013), or from higher frequency waves, as suggested by Takasuka et al. (2019) and (Wei et al., 2019). Future

work should examine in more detail the potential diversity in the atmospheric conditions that lead to MJO initiation, as also suggested by Li et al. (2015).

In summary, our results reveal that vertical moisture advection from adiabatic lifting plays an important role in MJO initiation. Because dry adiabatic lifting is intrinsically related to temperature tendencies in large-scale propagating waves, these results indicate that small departures from WTG balance may play an important role in the developing stages of the MJO. Thus, the conventional WTG approximation, which neglects small temperature fluctuations in the free troposphere, is not adequate at this time. While both the ERA-I and DYNAMO data show that dry adiabatic lifting plays an important role at this time, they disagree on whether dry adiabatic lifting plays a major role in moistening the troposphere prior to the onset of convection. More work is needed to further quantify the importance of dry adiabatic lifting during MJO initiation. Future work should also examine the role of dry adiabatic motions in the evolution of the MJO and other tropical motion systems. An improved understanding of such processes could lead to improvements in the modeling and prediction of tropical motions and its impact on the global climate system.

Chapter 5

Maritime Continent Initiation

5.1 Composite Primary and Successive Initiation

The analysis in Chapter 4 is repeated to determine key processes involved in MJO initiations that occur over the Maritime Continent (110°-160°E). Initiations in this region can be approximately described by MJO phase 3 and 4, which encompasses quadrant 'B' as identified in Fig. 5.1, which depicts primary and successive events. For primary events, the OMI index reaches a value of 0.8 at lag day 0 in quadrant 'B' with no prior activity beforehand. However, for successive initiation events the OMI index exceeds a value of unity for ~11 days prior to lag day 0 indicating MJO activity prior to initiation. The evolution is similar to those found over the Indian Ocean, which presented a slow decay.
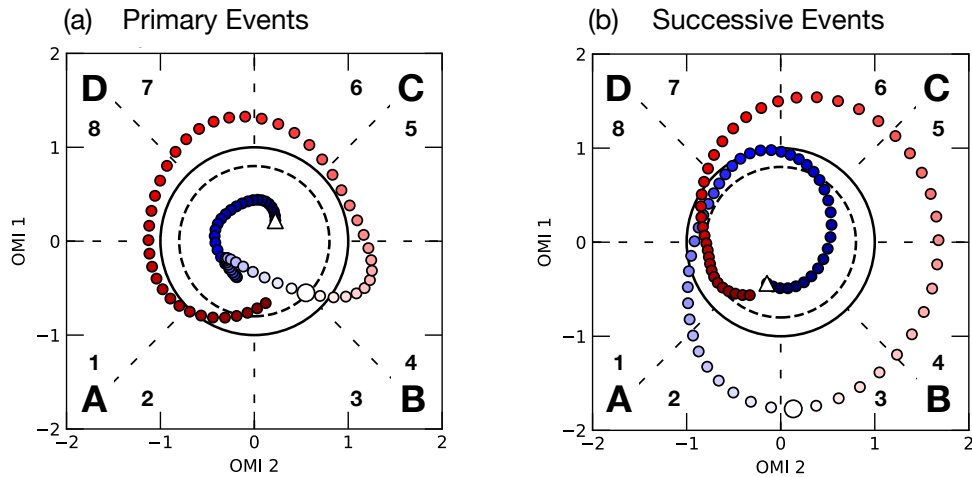
FIGURE 5.1: Composite phase space diagram of the OMI index for days -45 to 45 for (a) primary and (b) successive initiation events. The solid black circle represents an amplitude of 1.0. The dashed circle represents an amplitude of 0.8, the threshold necessary for events to not be categorized as 'N'. The white triangle marker denotes lag day -45 and the larger circle marker denotes lag day 0. The shading of the circles changes with increasing time, with darker blues indicating negative lags and reds indicating positive lags. The four quadrants and their corresponding MJO phases are shown in the corners of each panel.

Primary and successive initiation events can be looked at using a time-longitude diagram of OLR and χ anomalies as shown in Fig. 5.2a and 5.2b. During primary events, convection, as indicated by a negative OLR anomaly, begins around lag day -5 over the central portion of the Indian Ocean. By lag day 0, the negative OLR anomaly becomes a maximum at $\sim$100°E and is co-located with a negative 150-hPa χ anomaly that propagated from Africa. Both the OLR and χ anomalies can be seen propagating eastward but convection dies out around $\sim$180°E as it reaches the Pacific Ocean. At lag day 20, positive OLR anomalies build over the Maritime continent, indicating a suppressed phase of the MJO. Although Fig. 5.2b represents a Maritime Continent initiation, convection begins in the Indian Ocean with the strongest OLR anomalies lined up with Indonesia.

Unlike Indian Ocean initiations (Fig. 4.1), there is no significant suppressed convection to the west.

Unlike in primary initiation, there is evidence of previous MJO activity in Fig. 5.2b for the composited successive events. There is a propagating signal in the χ anomalies that can be traced back to lag day -45. At lag day -40 a negative OLR anomaly can be seen propagating eastward from the Indian Ocean which is associated with a prior MJO. The circumnavigating signal reaches its way back to the Indian Ocean near lag day 0, but convection begins over Africa at lag day -10. This signal continues propagating eastward but convection dampens near $\sim$180°E, similar to primary events.
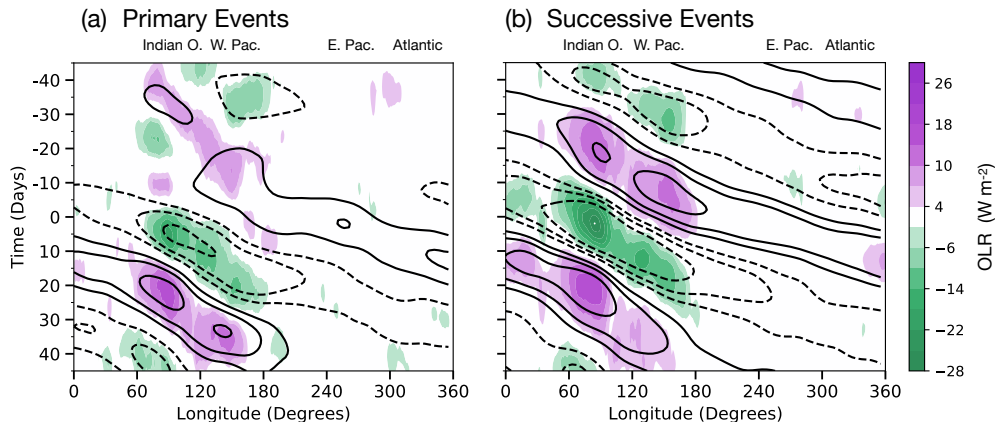
FIGURE 5.2: Hovmöller diagram of 20-100 day filtered anomalous outgoing longwave radiation (OLR) (shaded) and 150 hPa velocity potential (contoured) averaged over the 10°N/S latitude belt for (a) the lag composite of 25 primary MJO initiation events and (b) the composite of 52 successive initiation events. The ordinate shows the lag days from the time of initiation, with negative lags indicating days prior to the start of MJO initiation and positive lags indicating days after initiation. The contour interval is 10^5 m² s⁻¹.

The evolution of moisture as outlined in Eq. (3.5) is used to understand the processes involved in convection associated with MJO primary and successive initiation (Fig. 5.3).

In primary initiations, moistening begins near lag day -5 and slightly east of the Maritime Continent. There is about a 5 day lag between the moistening processes and the $\langle q \rangle$ anomalies which become a maximum at lag day 8 over Indonesia. The moistening tendency slowly propagates east until it reaches the Western Pacific Ocean.
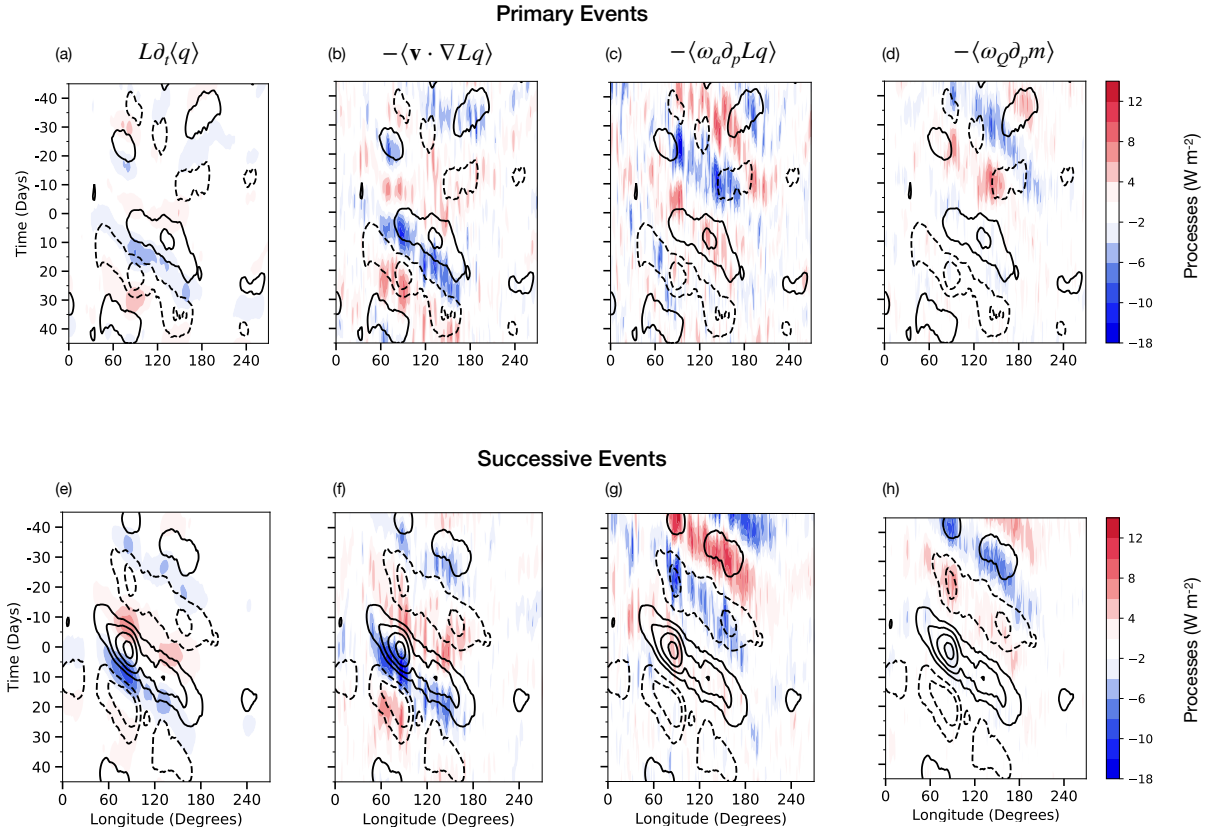
FIGURE 5.3: Hovmoller diagram of filtered (20-100 days) column integrated thermodynamic term anomalies (shading) and $\langle q \rangle$ anomalies (contoured) averaged over the 10°N/S latitude belt for both primary and successive events. (a) Moisture tendency term, (b) $-\langle \mathbf{v} \cdot \nabla Lq \rangle$, (c) $-\langle \omega_a \partial_p Lq \rangle$ and (d) $-\langle \omega_Q \partial_p m \rangle$. The contour interval for $\langle q \rangle$ is 0.5 mm.

Fig. 5.3b-d show the terms on the right-hand side of Eq. (3.5) which describes the processes leading to moistening. The horizontal moisture advection $(-\langle \mathbf{v} \cdot \nabla Lq \rangle)$ is largely in phase with the moisture tendency and is a precursor of the $\langle q \rangle$ anomalies.

This suggests that horizontal moisture advection is largely a propagation process unlike, $-\langle\omega_a\partial_p Lq\rangle$ and $-\langle\omega_Q\partial_p m\rangle$ which are in phase with the moisture anomalies. The adiabatic and diabatic processes are of opposite signs and tend to work against each other. A signal in $-\langle\omega_a\partial_p Lq\rangle$ can be roughly traced back to Africa around lag day -25 suggesting that it may aid in triggering convection during initiation. In contrast to adiabatic moistening, $-\langle\omega_Q\partial_p m\rangle$, contributes to drying due to moisture loss from condensation. However, it is slightly weaker than $-\langle\omega_a\partial_p Lq\rangle$ for primary initiations over the Maritime Continent.
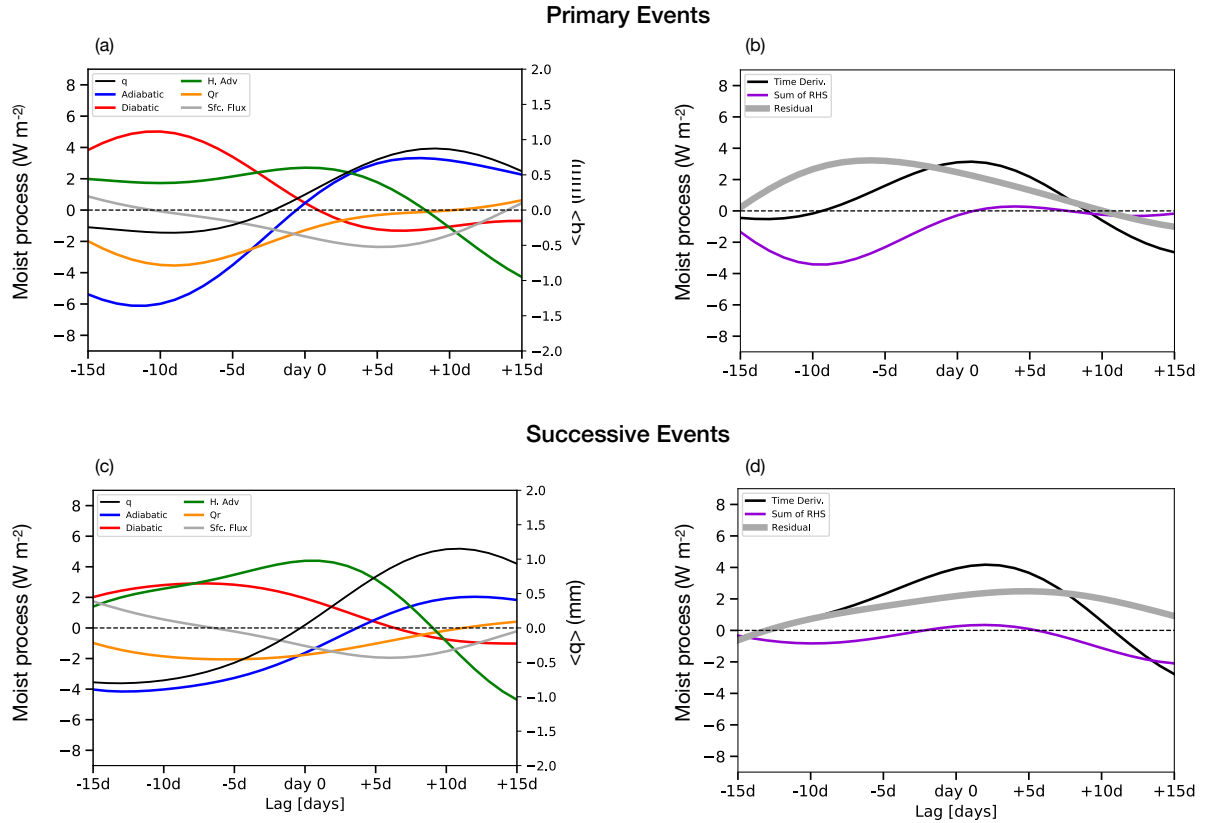
FIGURE 5.4: Lag composites of the column integrated moisture budget filtered for the MJO (20-100 days) and averaged over the Maritime Continent (10°N to 10°S and 110° to 160°) for (top) primary and (bottom) successive events. (a) Temporal evolution of $-\langle\omega_a\partial_p Lq\rangle$ (blue), $-\langle\omega_Q\partial_p m\rangle$ (red), horizontal moisture advection (green), radiative heating $\langle Q_r\rangle$ (orange) and column-integrated specific humidity (black). (b) Temporal evolution of the moisture tendency (black), the sum of all the right-hand-side terms in Eq. (3.5) (purple), and the budget residual (gray).

In contrast to primary initiations, the moisture evolution extends further west in successive events and a drying signal can be seen at lag day -35 which is associated with the circumnavigating signal. Similarly, there is about a 10 day lag time between the maximum in the moisture evolution and moisture anomalies between both primary and successive initiations. The $(-\langle \mathbf{v} \cdot \nabla Lq \rangle)$, is stronger in successive events due to the contribution of the circumnavigating signal causing easterly winds to advect moisture from the Maritime Continent. Overall $-\langle \omega_a \partial_p Lq \rangle$ and $-\langle \omega_Q \partial_p m \rangle$ are slightly weaker compared to primary events but follow a similar evolution.

The moist processes found in Fig. 5.3 are averaged over the Maritime Continent ($10°$N to $10°$S and $110°$ to $160°$E and are shown as a time evolution in Fig. 5.4. Initiation is defined at lag day 2 where the moisture tendency is at its maximum. In primary events, the horizontal moisture advection moistens the atmosphere prior to initiation, until lag day 2, where the term starts decaying and contributes to drying at lag day 8. As seen in Fig. 5.3., $-\langle \omega_a \partial_p Lq \rangle$ has a slightly larger amplitude but acts to cancel out the drying from $-\langle \omega_Q \partial_p m \rangle$. The $-\langle \omega_a \partial_p Lq \rangle$ peaks about 2 to 3 days after initiation and is in phase with the $\langle q \rangle$ anomalies. The sum of the terms on the RHS of the equation underestimate the moisture tendency leading to a residual term, as discussed in Chapter 4.

The successive initiations follow a similar evolution but with two key differences, $-\langle \mathbf{v} \cdot \nabla Lq \rangle$ is larger and $-\langle \omega_a \partial_p Lq \rangle$ is slightly smaller compared to primary events. Another difference is the timing in the $-\langle \omega_a \partial_p Lq \rangle$ term, which contributes to moistening 5 days

later and therefore peaks later in the evolution. Similarly, the sum of the RHS underestimates the moisture tendency and the terms largely cancel each other out.
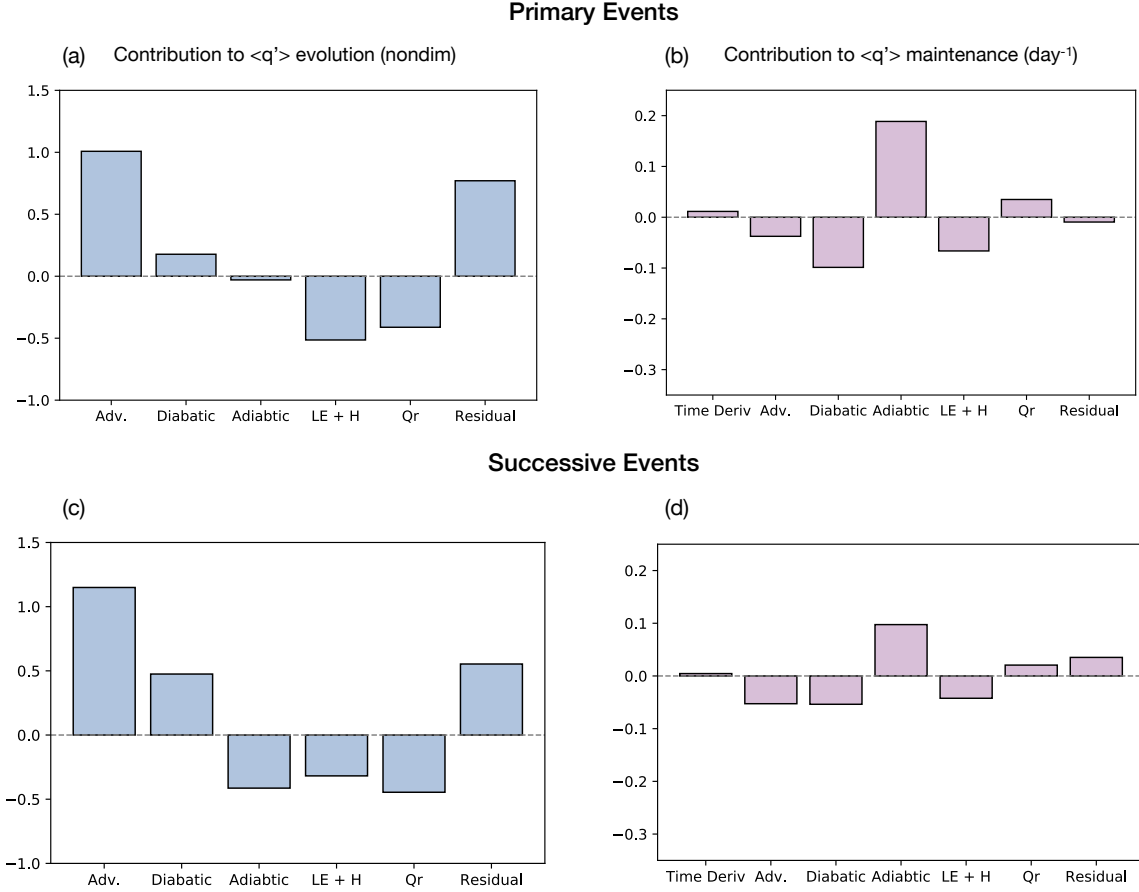
Primary Events

FIGURE 5.5: Fractional contribution of the thermodynamic budget in Equation (3.5) of moisture anomaly propagation and maintenance averaged over the Maritime Continent (10°N to 10°S and 110° to 160°E) for (a,b) primary events and (c,d) successive events. The projected terms are (from left to right): $\partial_t \langle Lq \rangle$, $-\langle \mathbf{v} \cdot \nabla Lq \rangle$, $-\langle \omega_Q \partial_p m \rangle$, $-\langle \omega_a \partial_p Lq \rangle$, $\langle Q_r \rangle$ and the budget residual.

Using Eq. 4.1, the contribution of the different processes to MJO maintenance and propagation can be determined. For both primary and successive initiation, the large-scale horizontal moisture advection is the strongest contributor to moisture propagation (Fig. 5.5a,c) associated with the MJO, while $-\langle \omega_Q \partial_p m \rangle$ is the second largest. In both

cases, the $-\langle \omega_a \partial_p Lq \rangle$, surface fluxes and $\langle Q_r \rangle$ negatively contribute to moisture evolution during initiation. However there is a large residual that represents error in the calculations and model parameterizations.

For MJO maintenance (Fig. 5.5.b,d), the $-\langle \omega_a \partial_p Lq \rangle$ is the strongest contributor in both cases but is much larger in primary events. This means that $-\langle \omega_a \partial_p Lq \rangle$ largely counteracts drying caused by condensation processes. It is important to note that $\langle Q_r \rangle$ contributes to moistening but plays a smaller role than dry adiabatic lifting. Overall the amplitude and sign of the rest of the terms are comparable across the board and a small residual is included.

5.2 Discussion

In this chapter, primary and successive MJO initiations over the Maritime Continent are investigated using a "relaxed WTG" moisture budget (Adames et al., 2021) as used in Chapter 4. The Maritime Continent was defined as quadrant 'B' in Fig 5.1, this includes MJO phase 2 and 3. It was found that large-scale horizontal moisture advection played a significant role in the moisture evolution for both primary and successive events, preceding the moisture anomalies. However, this process was about twice as strong in successive events primarily due to the circumnavigating signal causing anomalous easterlies. For primary events, horizontal moisture advection may be explained by the weak positive OLR anomaly prior to initiation leading to anomalous easterlies. A similar result was

found in Matthews (2008) noting that suppressed convection was a precursor to primary initiation events.

Vertical moisture advection by dry adiabatic motions was determined to play a non-negligible role during convective initiation of both primary and successive initiation events. Unlike horizontal moisture advection, dry adiabatic lifting was more important during convection, which made it the leading term in the moisture anomaly maintenance (Fig. 5.5b,d). This contribution was stronger in primary events by twice as much but was off set by a the larger vertical MSE advection term. Overall the evolution of moisture during primary and successive events followed a similar progression and highlighted the importance of dry adiabatic motions in maintaining and strengthening moisture anomalies associated with convection. These results suggest that small temperature fluctuations in the tropical atmosphere should not be neglected and the role of dry adiabatic motions should be further examined.

Comparing the results for the Maritime Continent to those over the Indian Ocean (Chapter 4) reveal many similarities and differences. A significant difference in both primary and successive events is the timing of the large-scale horizontal moisture advection term. For initiations over the Indian Ocean, the maximum of $-\langle \mathbf{v} \cdot \nabla Lq \rangle$ has a 15 day lag between the peak of the moisture anomalies. This lag time is significantly smaller for Maritime Continent initiations, with about a 5 to 8 day difference. This may have to do with the proximity of the moisture source between the two cases. Another key difference is the significance of $\langle Q_r \rangle$ between the two initiation locations. Over the Indian Ocean,

$\langle Q_r \rangle$ is important to the maintenance of moisture anomalies for both primary and successive events. This contrasts to initiations over the Maritime Continent where, $\langle Q_r \rangle$ plays a small and slightly negative role, this is possibly due to differences in how the convection is structured or represented in reanalysis. Lastly, the sign of $-\langle \omega_Q \partial_p m \rangle$ differed between locations in respect to its contribution to moisture anomaly evolution. This term negatively influenced moisture evolution over the Maritime Continent but because of the large residual it is difficult to say if this can be attributed to errors in model heating and will need to be further investigated. One hypothesis for the sign of this term is because of the large amount of moisture available over the Maritime Continent, the vertical advection of moisture from convective updrafts may outweigh moisture loss to condensation.

Despite these differences, large-scale horizontal moisture advection and dry adiabatic processes have a leading order of importance to MJO initiation. Furthermore, it is clear that dry adiabatic processes play a key role in the moistening processes of the MJO regardless of where convective initiation occurs. In both studies, dry adiabatic lifting was in phase with the moisture anomalies and largely contributed to maintenance processes (Fig 5.5 and Fig 4.5). Without this term, drying from condensation would dominate the moisture tendency causing the MJO to weaken. Overall these two studies are in agreement of key processes and the general evolution of primary and successive initiation events.

Chapter 6

Conclusions and Future Work

6.1   Conclusion

On the basis of a "relaxed WTG" approximation of the thermodynamic equation, the evolution of moisture can be manipulated in such a way to include adiabatic motions (Adames et al., 2021). The results of a scale analysis show that the vertical advection of moisture done by diabatic motions and those done by adiabatic motions are of similar magnitude. The conventional WTG approximations neglects the small tropical temperature fluctuations. In this study we hypothesize that these small temperature fluctuations are important to the moisture tendency and play a non-negligible role in the convective initiation of the MJO. In this study we quantified the leading order terms of the moisture equation for primary and successive events. Initiation is determined following the

methodology of Matthews (2008) and we apply this criteria for the Indian Ocean and Maritime Continent.

The results found in Chapter 4 and 5 suggest that dry adiabatic lifting is of leading order importance to the maintenance of moisture anomalies associated with the MJO. Although it is not analyzed in this study, the adiabatic signal is hypothesized to be associated with kelvin waves and/or extratropical influneces. Through this analysis, a general order of the processes that occur during the initiation period can be determined. Large-scale horizontal advection lead the moisture anomalies in all cases but are generally strongest for successive events, likely due to the circumnavigating signal creating anomalous easterlies at the surface. Once convection is initiated, dry adiabatic processes become important to maintain the moisture anomalies as they propagate eastward. For initiations over the Indian Ocean, $\langle Q_r \rangle$ plays a leading order role in anomaly maintenance but slows down propagation for the Maritime Continent. Furthermore, using observational data collected from the DYNAMO field campaign solidifies the results because of a negligible residual. In the DYNAMO analysis it was found that dry adiabatic motions are of leading order importance, and are of a comparable magnitude to large-scale horizontal moisture advection.

In conclusion, these results suggest that WTG approximation is not adequate for studying MJO initation because it neglects small temperature fluctuations and dry adiabatic processes as a result. This may also be the case for other tropical phenomena such as

equatorial rossby and kelvin waves. A "relaxed WTG" approach can further our understanding of how convection evolves in the tropics and provide a more complete picture.

6.2   Future Work

The MJO is a leading source of predictability on the subseasonal to seasonal (S2S) time frame, which describes the forecast period between two weeks to two months. Successful S2S forecasts are useful because they are able to provide information about tropical cyclone activity and extreme temperature events. Forecasts for this timescale are characterized by poor skill and low predictability and there are large socioeconomic decisions that could utilize forecast information in these mid-range timescales. It is especially important for emergency management mitigation because the slow onset of long-lasting events such as droughts and temperature extremes account for a large portion of weather-related disaster costs (Vitart, 2017). These medium range forecasts are difficult for two reasons: (1) the lead time is too long, meaning that initial conditions are generally lost and (2) oceanic processes vary too slowly to have a large influence on the S2S timescale. To tackle this issue, the framework provided in this study can be used on model reforecasts in the S2S Prediction Project Database to quantify the vertical moisture advection by adiabatic motions in both the forecasts and reforecasts. Statistics of the reforecasts from the different models should determine whether tropospheric moistening by adiabatic motions is an essential process for MJO initiation and to what degree models capture this process. A comparison of the numerous models should shed light on how MJO prediction can be improved during the crucial initiation stage.

Furthermore, model intervention experiments can be performed to test the degree to which dry adiabatic lifting plays a role in MJO predictability. Using reanalysis data, adiabatic motions can be calculated and used to correct the initial conditions of a given model. Understanding how the forecast changes based on how adiabatic motions are represented can be important to improving predictability.

Bibliography

Adames, Á. F., 2017: Precipitation budget of the madden-julian oscillation. *Journal of the Atmospheric Sciences*, **74**, 1799 – 1817, doi:10.1175/JAS-D-16-0242.1.

Adames, Á. F. and E. D. Maloney, 2021: Moisture Mode Theory's Contribution to Advances in our Understanding of the Madden-Julian Oscillation and Other Tropical Disturbances. *Current Climate Change Reports*, doi:10.1007/s40641-021-00172-4.

URL https://doi.org/10.1007/s40641-021-00172-4

Adames, Á. F., S. W. Powell, F. Ahmed, V. C. Mayta, and J. D. Neelin, 2021: Tropical precipitation evolution in a buoyancy-budget framework. *Journal of the Atmospheric Sciences*, doi:10.1175/JAS-D-20-0074.1.

Adames, Á. F. and J. M. Wallace, 2014: Three-dimensional structure and evolution of the mjo and its relation to the mean flow. *Journal of the Atmospheric Sciences*, **71**, 2007 – 2026, doi:10.1175/JAS-D-13-0254.1.

URL https://journals.ametsoc.org/view/journals/atsc/71/6/jas-d-13-0254.1.xml

Andersen, J. A. and Z. Kuang, 2012: Moist static energy budget of mjo-like disturbances in the atmosphere of a zonally symmetric aquaplanet. *Journal of Climate*, **25**, 2782 – 2804, doi:10.1175/JCLI-D-11-00168.1.

Bellenger, H., K. Yoneyama, M. Katsumata, T. Nishizawa, K. Yasunaga, and R. Shirooka, 2015: Observation of moisture tendencies related to shallow convection. *Journal of the Atmospheric Sciences*, **72**, 641 – 659, doi:10.1175/JAS-D-14-0042.1.
URL `https://journals.ametsoc.org/view/journals/atsc/72/2/jas-d-14-0042.1.xml`

Chen, X. and F. Zhang, 2019: Relative roles of preconditioning moistening and global circumnavigating mode on the mjo convective initiation during dynamo. *Geophysical Research Letters*, **46**, 1079–1087, doi:https://doi.org/10.1029/2018GL080987.

Chikira, M., 2014: Eastward-Propagating Intraseasonal Oscillation Represented by Chikira–Sugiyama Cumulus Parameterization. Part II: Understanding Moisture Variation under Weak Temperature Gradient Balance. *Journal of the Atmospheric Sciences*, **71**, 615 – 639, doi:10.1175/JAS-D-13-038.1.

Ciesielski, P. E., H. Yu, R. H. Johnson, K. Yoneyama, M. Katsumata, C. N. Long, J. Wang, S. M. Loehrer, K. Young, S. F. Williams, W. Brown, J. Braun, and T. Van Hove, 2014: Quality-Controlled Upper-Air Sounding Dataset for DYNAMO/CINDY/AMIE: Development and Corrections. *Journal of Atmospheric and Oceanic Technology*, **31**, 741–764.

Dee, D. P., S. M. Uppala, A. J. Simmons, P. Berrisford, P. Poli, S. Kobayashi, U. Andrae, M. A. Balmaseda, G. Balsamo, P. Bauer, P. Bechtold, A. C. M. Beljaars, L. van de Berg, J. Bidlot, N. Bormann, C. Delsol, R. Dragani, M. Fuentes, A. J. Geer, L. Haimberger, S. B. Healy, H. Hersbach, E. V. H??lm, L. Isaksen, P. K??llberg, M. K??hler, M. Matricardi, A. P. McNally, B. M. Monge-Sanz, J.-J. Morcrette, B.-K. Park, C. Peubey, P. de Rosnay, C. Tavolato, J.-N. Th??paut, and F. Vitart, 2011: The ERA-Interim reanalysis: configuration and performance of the data assimilation system. *Quart. J. Roy. Meteor. Soc.*, **137**, 553–597, doi:10.1002/qj.828.

Duchon, C. E., 1979: Lanczos Filtering in One and Two Dimensions. *Journal of Applied Meteorology*, **18**, 1016–1022.

Haertel, P., K. Straub, and A. Budsock, 2015: Transforming circumnavigating kelvin waves that initiate and dissipate the madden–julian oscillation. *Quarterly Journal of the Royal Meteorological Society*, **141**, 1586–1602, doi:https://doi.org/10.1002/qj.2461.

Hendon, H. H. and M. L. Salby, 1994: The Life Cycle of the Madden–Julian Oscillation. *Journal of Atmospheric Sciences*, **51**, 2225 – 2237, doi:10.1175/1520-0469(1994)051¡2225:TLCOTM¿2.0.CO;2.

Inoue, K., Á. F. Adames, and K. Yasunaga, 2020: Vertical velocity profiles in convectively coupled equatorial waves and mjo: New diagnoses of vertical velocity profiles in the wavenumber-frequency domain. *Journal of the Atmospheric Sciences*, **77**, 2139 – 2162, doi:10.1175/JAS-D-19-0209.1.

Inoue, K. and L. Back, 2015: Column-integrated moist static energy budget analysis on various time scales during toga coare. *Journal of the Atmospheric Sciences*, **72**, 1856 – 1871, doi:10.1175/JAS-D-14-0249.1.

Janiga, M. A. and C. Zhang, 2016: Mjo moisture budget during dynamo in a cloud-resolving model. *Journal of the Atmospheric Sciences*, **73**, 2257 – 2278, doi:10.1175/JAS-D-14-0379.1.

URL https://journals.ametsoc.org/view/journals/atsc/73/6/jas-d-14-0379.1.xml

Jiang, X., F. Adames, D. Kim, E. D. Maloney, H. Lin, H. Kim, C. Zhang, C. A. DeMott, and N. P. Klingaman, 2020: Fifty years of research on the madden-julian oscillation: Recent progress, challenges, and perspectives. *Journal of Geophysical Research: Atmospheres*, **125**, e2019JD030911, doi:https://doi.org/10.1029/2019JD030911.

Johnson, R. H., P. E. Ciesielski, J. H. Ruppert, and M. Katsumata, 2015: Sounding-Based Thermodynamic Budgets for DYNAMO. *J. Atmos. Sci.*, **72**, 598–622.

Kikuchi, K. and Y. N. Takayabu, 2003: Equatorial circumnavigation of moisture signal associated with the madden-julian oscillation (mjo) during boreal winter. *Journal of the Meteorological Society of Japan. Ser. II*, **81**, 851–869, doi:10.2151/jmsj.81.851.

Kiladis, G. N., J. Dias, K. H. Straub, M. C. Wheeler, S. N. Tulich, K. Kikuchi, K. M. Weickmann, and M. J. Ventrice, 2014: A comparison of olr and circulation-based indices for tracking the mjo. *Monthly Weather Review*, **142**, 1697 – 1715, doi:10.1175/MWR-D-13-00301.1.

Kiladis, G. N., K. H. Straub, and P. T. Haertel, 2005: Zonal and vertical structure of the madden–julian oscillation. *Journal of the Atmospheric Sciences*, **62**, 2790 – 2809, doi:10.1175/JAS3520.1.

Kim, D., M.-I. Lee, D. Kim, S. D. Schubert, D. E. Waliser, and B. Tian, 2014b: Representation of tropical subseasonal variability of precipitation in global reanalyses. *Climate Dyn.*, **43**, 517–534.

Kim, H., F. Vitart, and D. E. Waliser, 2018: Prediction of the madden-julian oscillation: A review. *Journal of Climate*, **31**, 9425 – 9443, doi:10.1175/JCLI-D-18-0210.1.

Kim, H., P. J. Webster, V. E. Toma, and D. Kim, 2014: Predictability and prediction skill of the mjo in two operational forecasting systems. *Journal of Climate*, **27**, 5364 – 5378, doi:10.1175/JCLI-D-13-00480.1.

Li, T., C. Zhao, P. chi Hsu, and T. Nasuno, 2015: Mjo initiation processes over the tropical indian ocean during dynamo/cindy2011. *Journal of Climate*, **28**, 2121 – 2135, doi:10.1175/JCLI-D-14-00328.1.
URL `https://journals.ametsoc.org/view/journals/clim/28/6/jcli-d-14-00328.1.xml`

Liebmann, B. and C. A. Smith, 1996: Description of a complete (interpolated) outgoing longwave radiation dataset. *Bulletin of the American Meteorological Society*, **77**, 1275–1277.
URL `http://www.jstor.org/stable/26233278`

Madden, R. A. and P. R. Julian, 1971: Detection of a 40-50 day oscillation in the zonal wind in the tropical pacific. *Journal of Atmospheric Sciences*, **28**, 702 – 708, doi:10.1175/1520-0469(1971)028¡0702:DOADOI¿2.0.CO;2.

— 1972: Description of global-scale circulation cells in the tropics with a 40-50 day period. *Journal of Atmospheric Sciences*, **29**, 1109 – 1123, doi:10.1175/1520-0469(1972)029¡1109:DOGSCC¿2.0.CO;2.

Mapes, B. E., 1997: *Mutual Adjustment of Mass Flux and Stratification Profiles*, Springer Netherlands, Dordrecht. 399–411.
URL `https://doi.org/10.1007/978-94-015-8828a7_16`

Mapes, B. E. and J. T. Bacmeister, 2012: Diagnosis of tropical biases and the mjo from patterns in the merra analysis tendency fields. *Journal of Climate*, **25**, 6202 – 6214, doi:10.1175/JCLI-D-11-00424.1.

Matthews, A. J., 2008: Primary and successive events in the madden–julian oscillation. *Quarterly Journal of the Royal Meteorological Society*, **134**, 439–453, doi:https://doi.org/10.1002/qj.224.

Mei, S., T. Li, and W. Chen, 2015: Three-type MJO initiation processes over the Western Equatorial Indian Ocean. *Advances in Atmospheric Sciences*, **32**, 1208–1216, doi:10.1007/s00376-015-4201-0.
URL `https://doi.org/10.1007/s00376-015-4201-0`

Milliff, R. F. and R. A. Madden, 1996: The Existence and Vertical Structure of Fast, Eastward-Moving Disturbances in the Equatorial Troposphere. *Journal of Atmospheric Sciences*, **53**, 586 – 597, doi:10.1175/1520-0469(1996)053¡0586:TEAVSO¿2.0.CO;2.

Nasuno, T., T. Li, and K. Kikuchi, 2015: Moistening processes before the convective initiation of madden-julian oscillation events during the cindy2011/dynamo period. *Monthly Weather Review*, **143**, 622 – 643, doi:10.1175/MWR-D-14-00132.1.

Powell, S. W., 2016: Updraft buoyancy within and moistening by cumulonimbi prior to mjo convective onset in a regional model. *Journal of the Atmospheric Sciences*, **73**, 2913 – 2934, doi:10.1175/JAS-D-15-0326.1.

— 2017: Successive mjo propagation in merra-2 reanalysis. *Geophysical Research Letters*, **44**, 5178–5186, doi:https://doi.org/10.1002/2017GL073399.

Powell, S. W. and R. A. Houze Jr., 2015: Effect of dry large-scale vertical motions on initial mjo convective onset. *Journal of Geophysical Research: Atmospheres*, **120**, 4783–4805, doi:https://doi.org/10.1002/2014JD022961.
URL https://agupubs.onlinelibrary.wiley.com/doi/abs/10.1002/2014JD022961

Ray, P. and C. Zhang, 2010: A case study of the mechanics of extratropical influence on the initiation of the madden–julian oscillation. *Journal of the Atmospheric Sciences*, **67**, 515 – 528, doi:10.1175/2009JAS3059.1.
URL https://journals.ametsoc.org/view/journals/atsc/67/2/2009jas3059.1.xml

Ren, P., D. Kim, M.-S. Ahn, D. Kang, and H.-L. Ren, 2021: Intercomparison of mjo column moist static energy and water vapor budget among six modern reanalysis products. *Journal of Climate*, **34**, 2977 – 3001, doi:10.1175/JCLI-D-20-0653.1.

Ruppert, J. H. and R. H. Johnson, 2015: Diurnally modulated cumulus moistening in the preonset stage of the madden–julian oscillation during dynamo. *Journal of the Atmospheric Sciences*, **72**, 1622 – 1647, doi:10.1175/JAS-D-14-0218.1.
URL https://journals.ametsoc.org/view/journals/atsc/72/4/jas-d-14-0218.1.xml

Sakaeda, N. and P. E. Roundy, 2015: The development of upper-tropospheric wind over the western hemisphere in association with mjo convective initiation. *Journal of the Atmospheric Sciences*, **72**, 3138 – 3160, doi:10.1175/JAS-D-14-0293.1.

— 2016: The development of upper-tropospheric geopotential height anomaly in the western hemisphere during mjo convective initiations. *Quarterly Journal of the Royal Meteorological Society*, **142**, 942–956, doi:https://doi.org/10.1002/qj.2696.

Sobel, A., S. Wang, and D. Kim, 2014: Moist static energy budget of the mjo during dynamo. *Journal of the Atmospheric Sciences*, **71**, 4276 – 4291, doi:10.1175/JAS-D-14-0052.1.
URL https://journals.ametsoc.org/view/journals/atsc/71/11/jas-d-14-0052.1.xml

Sobel, A. H. and D. Kim, 2012: The MJO-Kelvin wave transition. *Geophysical Research Letters*, **39**, doi:https://doi.org/10.1029/2012GL053380.

Sobel, A. H., J. Nilsson, and L. M. Polvani, 2001: The weak temperature gradient approximation and balanced tropical moisture waves. *Journal of the Atmospheric Sciences*, **58**, 3650 – 3665, doi:10.1175/1520-0469(2001)058¡3650:TWTGAA¿2.0.CO;2.

Straub, K. H., 2013: Mjo initiation in the real-time multivariate mjo index. *Journal of Climate*, **26**, 1130 – 1151, doi:10.1175/JCLI-D-12-00074.1.

Takasuka, D., M. Satoh, and S. Yokoi, 2019: Observational evidence of mixed rossby-gravity waves as a driving force for the mjo convective initiation and propagation. *Geophysical Research Letters*, **46**, 5546–5555, doi:https://doi.org/10.1029/2019GL083108.

Vitart, F., 2017: Madden—julian oscillation prediction and teleconnections in the s2s database. *Quarterly Journal of the Royal Meteorological Society*, **143**, 2210–2220, doi:https://doi.org/10.1002/qj.3079.

URL https://rmets.onlinelibrary.wiley.com/doi/abs/10.1002/qj.3079

Wei, Y., M. Mu, H.-L. Ren, and J.-X. Fu, 2019: Conditional nonlinear optimal perturbations of moisture triggering primary mjo initiation. *Geophysical Research Letters*, **46**, 3492–3501, doi:https://doi.org/10.1029/2018GL081755.

Wolding, B., 2013: *Moist static energy and the Madden-Julian oscillation: Understanding initiation, maintenance and propagation through the application of novel diagnostics*. Ph.D. thesis, Colorado State University.

Wolding, B. O., E. D. Maloney, and M. Branson, 2016: Vertically resolved weak tempera-
ture gradient analysis of the madden-julian oscillation in sp-cesm. *Journal of Advances
in Modeling Earth Systems*, **8**, 1586–1619, doi:https://doi.org/10.1002/2016MS000724.

Yanai, M., S. Esbensen, and J.-H. Chu, 1973: Determination of Bulk Prop-
erties of Tropical Cloud Clusters from Large-Scale Heat and Moisture Bud-
gets. *Journal of Atmospheric Sciences*, **30**, 611 – 627, doi:10.1175/1520-
0469(1973)030¡0611:DOBPOT¿2.0.CO;2.

Yokoi, S., 2015: Multireanalysis comparison of variability in column water vapor and
its analysis increment associated with the madden–julian oscillation. *J. Climate*, **28**,
793–808.

Yong, M. J., Y., 2016: Mechanistic analysis of the suppressed convective anomaly precur-
sor associated with the initiation of primary mjo events over the tropical indian ocean.
Climate Dynamics, **46**, 779–795, doi:https://doi.org/10.1007/s00382-015-2612-3.

Zhang, C., 2005: Madden-julian oscillation. *Reviews of Geophysics*, **43**,
doi:https://doi.org/10.1029/2004RG000158.

— 2013: Madden–julian oscillation: Bridging weather and climate. *Bulletin of the
American Meteorological Society*, **94**, 1849 – 1870, doi:10.1175/BAMS-D-12-00026.1.
URL https://journals.ametsoc.org/view/journals/bams/94/12/
bams-d-12-00026.1.xml

Zhao, C., T. Li, and T. Zhou, 2013: Precursor signals and processes associated with mjo initiation over the tropical indian ocean. *Journal of Climate*, **26**, 291 – 307, doi:10.1175/JCLI-D-12-00113.1.